The *E. coli* clamp loader sharply bends DNA to load β-clamp onto small gaps

Fengwei Zheng[1], Nina Y. Yao[2], Roxana E. Georgescu[2], Meinan Lyu[1],
Michael E. O'Donnell[2,*], and Huilin Li[1,3,*]
[1] Department of Structural Biology, Van Andel Institute, Grand Rapids, Michigan, USA.
[2] DNA Replication Laboratory and Howard Hughes Medical Institute, The Rockefeller University, New York, New York, USA
[3] Lead contact

[*] Correspondence should be addressed to M.E.O (odonnel@rockefeller.edu) or H.L (Huilin.Li@vai.org)

In brief: Zheng et al. discover that the bacterial clamp loader DnaX-complex has evolved a completely novel mechanism to load the DNA sliding β-clamp to nicks and small-gapped DNA for DNA damage repair.

Highlights

- Unlike RFC, the shoulder of bacterial DnaX-complex is not a dedicated DNA binding site.
- Unlike RFC, the DnaX-complex does not unwind small-gapped DNA to load the clamp.
- The β-clamp has evolved an external DNA binding site that is absent in PCNA.
- The β-clamp loading mechanism at nicks and small gaps is different from that of PCNA loading.

Abstract. DNA sliding clamps are used by the replication machines of all organisms, from bacteria to human. These clamps do not self-assemble onto DNA but require a multiprotein ATPase clamp loader that recognizes a DNA 3′-recessed end to open and close sliding clamps onto it. We find here that the mechanism of clamp loading onto small ssDNA gaps is profoundly different between bacteria and eukaryotes. The eukaryotic RFC clamp loader unwinds dsDNA from the 3′-recessed end to widen the ssDNA gap and also binds the 5′-recessed DNA end at an external "shoulder" site. In contrast, the bacterial DnaX-complex neither unwinds DNA nor stably binds DNA at the shoulder site. Instead, the bacterial β-clamp has evolved an external DNA binding site that enables the DnaX-complex to sharply bend a gapped DNA by 150° to insert it into the clamp. Small DNA gaps are frequently associated with DNA damage, and the clamps loaded at these sites likely function in DNA repair.

Introduction

In all cell types, bacteria, archaea and eukaryotes, the DNA replication machinery utilize ring shaped clamps that encircle duplex DNA and tether the replicative DNA polymerases (Pol) to DNA for rapid and processive synthesis[1-4]. This is readily apparent in the *E. coli* Pol III replication system in which circular clamps were discovered[1]. *E. coli* Pol III core, lacking a clamp, only proceeds one nucleotide(nt)/s, but upon engaging its β-clamp Pol III travels >500 nt/s with exceedingly high processivity (>5 kb)[1]. Circular sliding clamps do not get onto DNA by themselves; they require an ATP-driven clamp loader comprised of five AAA+ (ATPases Associated with diverse cellular Activities) motor subunits that spiral around 3′ DNA [3,4]. In *E. coli* the clamp is the β dimer and each protomer contains three domains having the same chain fold, giving the dimer a pseudo six-fold symmetry. The eukaryotic equivalent is the PCNA ring, a trimer in which each subunit has two domains with the same chain folds as the β domains and thus also form a pseudo six-fold symmetric ring [2,5,6].

The *E. coli* clamp loader motor pentamer consists of δ, δ′ and three subunits encoded by dnaX[7,8]. *E. coli dnaX* encodes two isoforms: the full-length product called τ, and a shorter version produced by a translational frameshift called γ[8]. In this report, we will refer to this pentameric clamp loader as the DnaX-complex. The *E. coli* clamp loader also contains two small non-motor subunits (not required for clamp loading), ψ and χ[8]. This seven-subunit clamp loader will be referred to here as the DnaX-holo-complex. The eukaryotic clamp loader equivalent to the DnaX-complex is the hetero-pentamer RFC (Replication Factor C)[4,9]. All five RFC motor subunits are distinct AAA+ family proteins, and show homology to one another, and to the bacterial DnaX-complex motor subunits. Both the DnaX-complex and RFC structures have previously been solved by crystallography[7,10]. The pentameric 3D structures of the DnaX-complex and RFC are also quite similar; they are spirals that form an internal chamber that holds dsDNA, and each pentamer has a prominent gap between two motor subunits through which DNA can pass into their "internal chamber". The DNA clamp is located directly underneath the DNA binding internal chamber, explaining how clamp loaders position DNA through their requisite clamp[3]. Another shared feature is that the ATP sites are located at subunit interfaces, common to AAA+ oligomers, presumably for inter-subunit communication during the ATP hydrolysis and clamp loading process[3,11].

Clamp loading at a large gap (e.g., between Okazaki fragments) is well understood for both eukaryotic RFC loader[12-15] and the bacterial DnaX-complex[16,17]. In both cases, the clamp remains closed in solution until a clamp loader binds the clamp and pries it open[18]. A minor difference exists in that DnaX-complex moves counterclockwise to open the β-clamp, whereas RFC moves clockwise to open the PCNA[16], consistent with earlier biochemical studies that provided evidence for the opposite directionality of clamp opening by bacterial and eukaryotic clamp loaders[19,20]. Next, the DNA 3′-end enters and is specifically recognized by the chamber of the clamp loader, followed by dsDNA entering the chamber of the clamp

and the subsequent closure of the clamp around the dsDNA. These events only require ATP binding, not ATP hydrolysis[16,17,21]. Finally, biochemical studies have shown ATP hydrolysis in the clamp loader ejects the loader from the clamp to complete clamp loading[22-24].

Biochemical studies show that both the bacterial DnaX-complex and eukaryotic RFC can load their respective clamp at a nick or small gap (< 6 nt) for DNA repair. Clamp loading at a nick or small gap is more challenging and is an active area of research. The eukaryotic RFC was found to unwind from the 3′ end to widen a small gap[12-15]. RFC was also shown to possess an external "shoulder" 5′ DNA binding site formed by the unique Rfc1 BRCT domain and the Rfc1 AAA+ domain[12-15]. Therefore, RFC binds both the dsDNA with 5′-recessed end (hereafter 5′-dsDNA) and the dsDNA with 3′-recessed end (hereafter 3′-dsDNA), with the 5′-dsDNA at the external shoulder site and the 3′-dsDNA inside the RFC chamber[25-27].

How the bacterial DnaX-complex loads sliding clamps onto a nick or small gap has not been visualized (**Figure 1A**). Therefore, it has been unclear if DnaX-complex possesses an external DNA binding site and if DnaX-complex can unwind the primer 3′-end in a manner that resembles RFC. We have addressed these questions in the current study using DNA substrates bearing a small gap of 1 nt or a larger gap of 10 nt. We captured a total of 13 clamp loading intermediates and found that DnaX-complex neither unwinds DNA nor stably binds 5′-dsDNA at the shoulder site. Instead, the bacterial loader has evolved a totally novel DNA bending strategy to load the β-clamp to the small gaps.

RESULTS

1. β-clamp loading by DnaX-complex at a DNA nick

The *E. coli dnaX* gene encodes two isoforms, the full-length protein τ and a C-terminally truncated protein γ. Therefore, the seven-protein bacterial loader complex has two versions, containing either the pentameric $\tau_3\delta\delta'$ or $\gamma_3\delta\delta'$, plus the associated heterodimeric ψχ (**Figure 1B and S1**)[28]. We used the full-length version ($\tau_3\delta\delta'\psi\chi$, i.e. "τ-complex") for cryo-EM study and the truncated version ($\gamma_3\delta\delta'$ ψχ, "γ-complex") for biochemical study. Because previous studies showed that the *E. coli* DnaX-complex can load clamps onto nicked sites[1], we asked if the bacterial loader can unwind DNA (**Figure 1A**), just like the eukaryotic RFC that has been established to contain a true separation pin that unwinds the DNA 3′-recessed end to load PCNA onto a nick or small gapped DNA[13-15].

The amino acid in the *E. coli* DnaX-complex equivalent to the DNA-unwinding separation pin W638 of the yeast Rfc1 is the δ-subunit Y316. We purified the wildtype (WT) and the separation pin mutated (Y316A, Mut) DnaX-complexes and compared their β-clamp loading activities with plasmids having either a 20-nt gap or just a nick (0-nt, no gap) (see details in **STAR METHODS**). We found that the WT DnaX-complex loaded the β-clamp onto the 20-nt gapped and nicked plasmids with comparable efficiency (**Figure 1C**),

while the separation pin Y316A-mutant complex was substantially reduced in clamp loading efficiency on plasmid with a nick compared to full activity on a plasmid with a 20-nt gap. This finding suggested that the Y316 residue is functional in efficient clamp loading at nicks, which we presumed might be strand unwinding given the several studies of RFC showing unwinding of 3′-recessed ends. We next carried out cryo-EM analysis of DnaX-complex loading β-clamp onto a 1-nt gapped DNA, to examine if DNA unwinding indeed occurs.

2. Cryo-EM of bacterial DnaX-complex with a 1-nt gapped DNA

Studies of eukarytotic RFC demonstrated that a minimum of a 6-nt gap is required for RFC to thread through the interior chamber of the clamp loader, and upon encountering a gap smaller than this, RFC unwinds the 3′-end of DNA to widen the ssDNA gap. To understand why the mutant separation pin Y316A DnaX-complex is deficient in loading β onto nicked DNA (e.g. **Fig. 1c**), and to gain insight into how DnaX-complex loads the β-clamp onto small gaps (<6) (e.g. does it unwind DNA like RFC?), we assembled in vitro loading intermediates by mixing purified τ-complex, β-clamp, and a 1-nt gapped DNA at a stoichiometry of 1:1.3:1.5 in the presence of 5 mM Mg^{2+} and 0.5 mM ATPγS, a slowly hydrolyzable ATP analog[29] (**Figure 1D**). Cryo-grids were prepared with the mixture for cryo-EM structural analysis (**STAR METHODS)**.

Cryo-EM captured two major loading states in which the loading process is either just getting started or has largely completed (**Figures S2–3**, **Table 1**). In the first state, the β-clamp is open, but the 3′-dsDNA has yet to enter the β-clamp (**Figure 1E**). The 3′-recessed end is inside the loader chamber pointing to the δ-subunit Y316, but the 3′-dsDNA tilts 52° outwards away from β-clamp, but it is not inside β, and its rests instead on the outer surface of the open clamp gate. We have termed this intermediate the “DNA 3′-end recognition state”. Such 3′-dsDNA pose is unprecedented. In all structurally visualized clamp loading intermediates so far – prokaryotic or eukaryotic, the 3′-dsDNA is either invisible or has fully entered the clamp chamber. Therefore, this DNA 3′-end recognition state is novel and might be unique to the bacterial clamp loading system (described below).

The 5′-dsDNA had very weak density around the shoulder region of the DnaX-complex (**Figure 1E**). Further 3D classification resulted in three 3D maps in the resolution range of 3.14 to 2.71 Å. These three conformers differ in the 5′-dsDNA region (**Figures S2–3**). The ordered region of the 5′-dsDNA is 9 bp long in conformer 1, 5 bp long in conformer 2, and 0 bp (disordered) in conformer 3 (**Figure 1E**). Conformer 1 with largely ordered 5′-dsDNA accounts for only 6% of the particle population in this state, indicating that the DnaX-complex does not stably bind the 5′-dsDNA at the shoulder. In all three conformers of the first state, the separation pin residue δ Y316 is 3.3 to 5.0 Å away from the 3′-recessed end, but no strand separation or DNA unwinding has occured (**Figure 1E**). This finding is rather

141 surprising, because the analogous residue in eukaryotic RFC can unwind the 3′-end up to 6 bp, as
142 shown in both human and yeast systems[13-15,30].
143
144 Interestingly, the β-clamp gate opens by 28 Å (**Figure 1F**), wider than the previously observed 20 Å
145 openning when complexed with a tailed DNA[16]. The wider openning may be stabilized by the interaction
146 with the blunt end of the 3′-dsDNA.
147
148 **3. The DnaX-complex sharply bends DNA to load β-clamp onto 1-nt gapped DNA**
149 In the second major state, the 3′-dsDNA has fully entered the chambers of both the loader and clamp, so
150 it is a post loading state. Further classification of this state resulted in two conformers at a resolution of
151 2.72 Å and 3.12 Å, respectively. These conformers differ in the width of the β-clamp gate and the DNA
152 position (**Figures 2A, S2**–**3**). In conformer 1, the β-clamp gate is narrowed to 24 Å from the 28 Å in state
153 1, and the 5′-dsDNA bends downward by 150° to bind the β-clamp at the location that was previously
154 occupied by the 3′-dsDNA in state 1, as described above. In conformer 2, the 3′-dsDNA is inside the β-
155 clamp, the 5′-dsDNA bends less (137°) and dissociates from the β-clamp, and the clamp opening
156 narrows to 17 Å. These two conformers immediately suggest a clamp loading mechanism in which the
157 the 5′-dsDNA bends down to push the 3′-dsDNA into the β-clamp chamber (**Figure 2B**–**C**).
158
159 The eukaryotic RFC loads PCNA onto small gapped DNA by: (1) unwinding DNA from the 3′-end to
160 widen the gap, (2) binding and stabilizing both 3′-dsDNA and 5′-dsDNA (**Figure 2D**). We have shown
161 here that the bacterial clamp loader neither unwinds DNA nor stabily binds the 5′-dsDNA at the shoulder
162 site. Instead, the DnaX-complex loads β-clamp to the 1-nt gapped DNA via a DNA bending mechanism.
163 To our knowledge, such DNA bending mechanism is unprecedented and has not been observed
164 previously (**Figure 2D**).
165
166 **4. Cryo-EM of β-clamp loading intermediates on a 10-nt gapped DNA**
167 The unique DNA bending mechanism observed with the 1-nt gapped DNA relies on two features in the
168 bacterial clamp-clamp loader system: (1) the basic outer surface patch on the β-clamp that can bind and
169 transiently hold the duplex of the 3′-dsDNA, and (2) the shoulder site of the DnaX-complex does not
170 stably bind the 5′-dsDNA, such that the 5′-dsDNA can bend down towards, and force, the 3′-dsDNA to
171 enter the β-clamp chamber. We asked if the basic patch on the β-clamp is also used when loading the
172 clamp onto a ssDNA gap that is long enough to thread the clamp loader. To address this question, we
173 performed cryo-EM on the in vitro β-clamp loading intermediates with a 10-nt gapped DNA (**Figure 3A**).
174
175 Cryo-EM image processing resulted in eight 3D EM maps, likely corresponding to eight distinct clamp-
176 loading intermediates. The first map at 2.95 Å contains only the clamp loader but no β-clamp or DNA

177 substrate. This structure was observed previously and will not be further discussed here[7,31]. The
178 remaining seven maps contain both β-clamp and DNA substrate in a resolution range of 2.53 Å to 2.88 Å
179 (**Figures S4–5, Tables 1** and **S2**). These maps all had a peripheral fuzzy density visible at a lower
180 display threthold for the SSB-binding ψχ dimer (**Figure 3B** and **S4**) but contained no density for the C-
181 terminal domain of the three τ proteins, consistent with previous studies[16,17]. Therefore, these atomic
182 models contain only the γ-region, despite the use of the full-length τ in the structural study. To distinguish
183 from the reported crystal structures of the γ-complex ($\gamma_3\delta\delta'$) [7,31], we refer to the pentameric $\tau_3\delta\delta'$ as the
184 DnaX-complex and the heptameric $\tau_3\delta\delta'\psi\chi$ as the DnaX-holo-complex (**Figure 3C**).
185
186 The ψχ dimer structure was previously determined by X-ray crystallography[32]. A small angle X-ray
187 scattering study showed that ψχ dynamically associates with the top collar domain of the DnaX-complex
188 [33]. Furthermore the crystal structure of a ψ-peptide bound to the $\gamma_3\delta\delta'$ complex was also reported[31]. But
189 how ψχ associates with the pentameric DnaX-complex to assemble the heptameric holo-complex has
190 been unclear. Via local masking and focused refinement, we obtained a 5.5-Å EM map for the ψχ and
191 merged it with the first clamp-loading intermediate (**Figure S4**). The ψχ density fits well with the reported
192 crystal structure and, as expected, binds the DnaX-loader collar domain via the ψ subunit. Thus, the
193 composite map provides the first view of the DnaX-holo-complex (**Figures 3C** and **S4**).
194
195 **5. The basic patch on the β-clamp is utilized in clamp loading onto a 10-nt gapped DNA**
196 In the first loading intermediate with the 10-nt gapped DNA, the 5′-dsDNA is invisible, presumably mobile
197 outside the clamp–clamp loader complex. The DNA 3′-end is 3.5 Å away from but is not unwound by the
198 δ Y316 "separation pin" (**Figure 3C–D**). The 3′-dsDNA binds outside the open-gate β-clamp, resembling
199 state 1 with the 1-nt gapped DNA described above (**Figure 3C–D**). The 3′-dsDNA blunt end is stabilized
200 outside the clamp by the basic patch formed by R96, R103, and R105 (**Figures 3D–E** and **S6A**).
201 Structural-based sequence alignment amongst bacterial β-clamps with a sequence identity varying from
202 29% to 96% revealed a high conservation of the three arginine residues (**Figure S6B**), consistent with
203 their role in the clamp loading process. Importantly, the basic patch is unique to β-clamp and is absent in
204 PCNA (**Figure 3E**).
205
206 To further examine their functional importance, we mutated these arginines either to three alanines or
207 three aspartic acids, and incorporated a short N-terminal peptide ^{32}P-labeling motif in the wildtype (wt)
208 and mutant β-clamps to quantify their relative in vitro loading efficiency using the γ-complex, which loads
209 the β-clamp as efficiently as the τ-complex[19,34-36] (see **STAR METHODS**). We confirmed by mass
210 photometry that the two β-clamp mutants remained dimeric in solution (**Figure S6C**). We found that the
211 two triple mutant β-clamps were loaded by the DnaX-complex only half as efficiently (80 fmol) as the wt

212 β-clamp (160 fmol) (**Figure 3F**). This data is consistent with a functional role of the conserved basic
213 patch on the outer surface of the β-clamp.
214
215 **6. The intermediates depict a complete clamp-loading cycle**
216 The eight EM maps with the 10-nt gapped DNA describe a nearly full clamp-loading cycle (**Figures**
217 **S4**–**5**). Among these structures, six ternary clamp loader–clamp–DNA intermediates show how the clamp
218 gate transitions from fully open to fully closed to encircle DNA (**Figure 4A**–**B, Supplemental video 3**).
219 These intermediates are consistent with, and are complementary to the recently reported *E. coli* DnaX-
220 complex clamp loading intermediates with tailed DNAs[16,17]. The observed sequential loading process
221 resembles the eukaryotic PCNA and 9-1-1 clamp loading by the RFC and Rad24-RFC loader,
222 respectively[13-15,29].
223
224 The clamp loader region of the six loading conformers are similar, with an $RMSD_{Ca}$ ranging from 0.5 to
225 0.7 Å (**Figure 4A**–**B**). In the 1st conformer, the β-clamp gate is open by 22 Å, wide enough for passage of
226 the 20-Å wide dsDNA, and the 3′-dsDNA has entered the clamp but is tilted by 22° and has yet to settle
227 into the central chamber. This conformer is referred to as "fully open DNA unsettled" (**Figure 4A**). In the
228 2nd conformer, the DNA is less tilted (17°), and this conformer is referred to as "fully open DNA settled".
229 In the 3rd conformer, the clamp gate narrows to 8.5 Å and DNA is 16° tilted. In the 4th to 6th conformers,
230 the clamp gate becomes fully closed, and the β-clamp gradually dissociates from the DnaX-complex, by
231 tilting away by 4° from the 4th to 5th conformer, and by a further 3° from the 5th to the 6th conformer
232 (**Figure 4B**). From the DNA recognition conformer (state 1) to the gate partially-closed conformer (state
233 2), the interface between subunit DnaX3 and β-2 slightly increases from 958 $Å^2$ to 1097 $Å^2$, then
234 diminishes to 767 $Å^2$, 613 $Å^2$ and 0 $Å^2$ (no contact) in the following three gate fully-closed conformers,
235 respectively. The interface between subunit δ′ and β-2 is the same among the first four conformers (~950
236 $Å^2$), then drops to 340 $Å^2$ in the fully closed conformer 1, and with no interaction (0 $Å^2$) in the fully closed
237 conformer 2 and 3 (**Figure 4B**).
238
239 **7. The DNA 5′-end does not stimulate clamp loading activity of DnaX-complex**
240 The eukaryotic RFC clamp loaders have a highly positively charged shoulder that stably binds 5′-
241 dsDNA[29]. Unlike RFC, the 5′-dsDNA is largely disordered at the shoulder of the bacterial DnaX-complex
242 (**Figures 3**–**4**). We found the DnaX-complex shoulder is largely neutral and even somewhat negatively
243 charged, and may therefore be incapable of binding DNA stably (**Figure 5A**).
244
245 The absence of a dedicated shoulder DNA binding site predicts that the loading activity of DnaX-complex
246 is not facilitated by the presence of a 5′-recessed end. To test this prediction, we performed a
247 fluorecence polarization-based binding assay to determine RFC-DNA affinity using Cy3 labled DNA at a

248 3′ end (see details in **STAR METHODS**)[13] and compared the wild-type γ-complex with three different
249 DNA substrates: 1) a tailed DNA with only a recessed 3′-end, 2) a 10-nt gapped DNA with both recessed
250 3′- and 5′-end, and 3) a 30-nt gapped DNA (**Figure 5B**). We found that the apparent equilibrium
251 dissociation constant ($^{App}K_d$) is 117.8 ± 11.1 nM with the first substrate, 97.2 ± 13.7 nM with the second
252 substrate, and 93.7 ± 6.7 nM with the third substrate. These affinities are highly similar, inidicating that
253 the presence of a recessed 5′-end does not enhance DNA binding to the clamp loader, consistent with
254 the lack of a dedicated shoulder DNA-binding site in the *E. coli* clamp loader.
255
256 We further performed a clamp loading-dependent primer extension assay using two p/T substrates: a
257 tailed DNA with a 30-nt primer (Pri-1) annealed to a 100-nt template with biotin labelled at both ends and
258 with a ^{32}P-labelled 5′-end, and a 45-nt gapped DNA with an additional 25-nt primer (Pri-2). Streptavidin
259 (SA) was added to block the DNA blunt ends to prevent the β-clamp from diffusing off DNA (**Figures 5C**
260 and **S7**). Sufficient polymerase (Pol) III was added to ensure the reaction is rate-limited only by clamp
261 loading. The singly- and doubly-primed p/T were not extended by Pol III in the absence of clamp loading
262 under our conditions, and these served as negative controls. Both p/T substrates were extended in the
263 presence of clamp loading. We found the amount of synthesized DNA is similar with both substrates,
264 with the singly-primed p/T yielding a slightly higher amount (**Figure 5C**). This result is again consistent
265 with the structural observation that the *E. coli* clamp loader has no dedicated shoulder binding site for the
266 5′-dsDNA.
267
268 **DISCUSSION**
269 In this work, we have discovered a profound difference between the bacterial and eukaryotic clamp
270 loading onto nicks and small gapped DNAs. A minimum stretch of 6-nt ssDNA is requried to thread
271 through the loader chamber to enable the recognition and binding of the DNA 3′-end for clamp loading.
272 To load the clamp onto a small gap (< 6 nt), the eukaryotic RFC unwinds the DNA 3'-end to widen the
273 gap. The bacterial DnaX-complex instead bends the 5′-dsDNA by 150º toward the 3′-dsDNA, forcing the
274 3′-dsDNA into the clamp chamber without unwinding a single base. Despite the lack of unwinding
275 activity, the δ Y316 approaches and interacts with the DNA recessed 3′-end. We suggest that δ Y316
276 functions in recognition but not in unwinding of the DNA recessed 3′-end. The *E. coli* β-clamp has been
277 shown to function in DNA damage repair with TLS Pols[37-47]. Thus, the bending mechanism is likely
278 utilized for repairing damaged DNA with small gaps. Further investigation is needed to understand the
279 physiological consequences of conditions under which such DNA bending is utilized.
280
281 **Proposed β-clamp loading mechanism by DnaX-complex**
282 The bacterial clamp loader may load the β-clamp in a DNA structure-dependent manner. During normal
283 bacterial replication, a typical Okazaki fragment is 1–2 kb long, such that the preceding Okazaki fragment

284 (i.e., 5′-dsDNA) is too far away to influence the loading process and can essentially be ignored. We
285 propose that the 3′-dsDNA first binds in a tilted manner to the basic patch outside the open-gate β-clamp
286 (**Figure 6**). Next, the DnaX-complex readily engages the primer 3′-end via the δ Tyr-316 to enable the 3′-
287 dsDNA to diffuse toward the higher affinity site in the β-clamp chamber in a series of steps captured here
288 as well as in recent studies[16,17]. However, when it encounters a small gap (< 6 nt), arisen perhaps from
289 DNA damage or as a repair intermediate[45,48,49], the DnaX-complex needs a new strategy to load the β-
290 clamp, such that the sliding clamp will go on to recruit the Y-familiy polymerases (Pol II, IV, V) for gap
291 filling or translesion synthesis[45,50-52].
292
293 At a small gap, the primer 3′-end is initially obstructed from entering the DnaX-complex chamber,
294 because the adjacent 5′-dsDNA is too bulky to enter the chamber itself. In this case, 5′-dsDNA, not being
295 held in place by the DnaX-complex shoulder, bends down towards the 3′-dsDNA (**Figure 6**). The sharp
296 bending has two consequences: exposing the primer 3′-end to allow it to enter the DnaX-complex
297 chamber; generating stress in the U-shaped DNA to push the 3′-dsDNA away from the clamp external
298 site and towards the clamp chamber. This is followed by the 5′-dsDNA binding to the clamp basic patch
299 that has just been vacated by the 3′-dsDNA. Such 5′-dsDNA binding will further push the 3′-dsDNA into
300 the β-clamp chamber. The negatively charged DNA phosphate backbone will then attract the positively
301 charged chamber surface to close the β-clamp gate, similar to the gate closure mechanism proposed for
302 the PCNA and 9-1-1 clamp[12-15,25-27,29]. Once the DNA is fully encirlced by the β-clamp, ATP hydrolysis by
303 the DnaX-complex will dissociate the loader from the β-clamp[18]. We envision the U-shaped DNA will then
304 relax and resume a linear structure, now encircled by the β-clamp.
305
306 **The β-clamp external DNA binding site compensates for the lack of shoulder DNA site in DnaX-**
307 **complex**
308 Two DNA binding sites may be needed to sharply bend a DNA. For example, the yeast replication origin
309 DNA is bent 50º by the origin recognition complex (ORC, Orc1-6), with one DNA binding site inside the
310 ORC ring, and the other site on the surface formed by Orc5 and Orc6[53,54]. The eukaryotic RFC utilizes
311 two dsDNA binding sites to load PCNA onto gapped DNA: the primary site composed of the RFC internal
312 chamber (for the 3′-dsDNA), and a secondary site at the external shoulder (for the 5′-dsDNA). The RFC
313 shoulder is highly positively charged and stably binds the 5′-dsDNA[13,15,25-27], but the DnaX-complex
314 shoulder is not highly positively charged and the 5′-dsDNA is not stably bound there (**Figure 5A**).
315 Perhaps as a compensation for the lack of the shoulder DNA site in DnaX-complex, the β-clamp has
316 evolved a basic patch on the external surface to stably bind DNA, providing the second DNA binding site
317 for the bacterial clamp–clamp loader system (**Figures 3E** and **S6A**).
318
319 **DnaX-complex is anchored to the replication fork for repeated clamp loading**

320 The DnaX-complex is more than a clamp loader, as it organizes the major protein actors (helicase,
321 polymerases, and primase) at a DNA replication fork and potentially synchronizes the leading and
322 lagging strand DNA synthesis[55-58] (**Figure S8**). Such extraordinary ability is conferred by the flexiblly
323 linked CTD of the three τ subunitis (τ_{CTD}) of the DnaX-complex[59], with one CTD anchoring the leading
324 strand Pol, another CTD the lagging strand Pol, and the remaining CTD a third Pol at the fork[60,61]. The
325 DnaX-complex also anchors the replisome to the replication fork via its χ subunit that binds to the ssDNA
326 binding protein SSB[32,56]. We have visualized for the first time the ψχ sitting atop the DnaX-holo-complex
327 (**Figure S8**). The ability to bind the SSB on ssDNA may explain the observations of how the χ subunit
328 facilitates clamp loader function to load the β-clamp to the primer 3′-end.
329
330
331 **STAR★METHODS**
332 Detailed methods are provided in the online version of this paper and include the following:
333 - KEY RESOURCES TABLE
334 - RESOURCE AVAILABILITY
335 - Lead contact
336 - Materials availability
337 - Data and code availability
338 - EXPERIMENTAL MODEL AND SUBJECT DETAILS
339 - METHOD DETAILS
340 - Protein expression and purification
341 - β-clamp mutants preparation
342 - γ-complex mutant preparation
343 - Gel filtration-based analysis of β-clamp loading
344 - Fluorescence polarization-based DNA binding assay
345 - Rate of clamp loading onto primed versus gapped DNA
346 - Cryo-EM grids preparation and data collection
347 - Image processing and 3D reconstruction
348 - Model building, refinement, and validation
349 - QUANTIFICATION AND STATISTICAL ANALYSIS
350
351 **SUPPLEMENTAL INFORMATION**
352 Supplemental Information can be found online at:
353
354 **ACKNOWLEDGMENTS**

Cryo-EM micrographs were collected at the David Van Andel Advanced Cryo-Electron Microscopy Suite in Van Andel Institute. We thank G. Zhao and X. Meng for facilitating data collection. This work was supported by the US National Institutes of Health grants GM115809 (to M.E.O.) and GM131754 (to H.L.) and the Howard Hughes Medical Institute (to M.E.O.) and the Van Andel Institute (to H.L.).

AUTHOR CONTRIBUTIONS

F.Z., M.E.O., and H.L. designed research; F.Z., R.E.G., N.Y., and M.L. performed research; F.Z., R.E.G., N.Y.Y., M.L., M.E.O., and H.L. analyzed the data; F.Z., M.E.O., and H.L. wrote the manuscript with input from all authors.

DECLARATION OF INTERESTS

The authors declare no competing interests.

368 **STAR★METHODS**

369 **KEY RESOURCES TABLE**

REAGENT or RESOURCE	SOURCE	IDENTIFIER
Antibodies		
Bacterial and virus strains		
E. coli DH5α competent cells	Thermo Fisher Scientific	Cat# 18265017
E. coli BL21(DE3) competent cells	Thermo Fisher Scientific	Cat# EC0114
Chemicals, peptides, and recombinant proteins		
dNTPs	Cytiva	Cat# 28406551
[γ-^{32}P] ATP	PerkinElmer Life Sciences	Cat# BLU002Z500UC
ATPγS	Millipore Sigma	Cat# 11162306001
Anti-FLAG beads	Millipore Sigma	Cat# A36797
Bradford protein assay kit	Bio-Rad	Cat# 5000001
Deposited data		
Cryo-EM map of DnaX-complex–β-clamp–1-nt gapped DNA at state 1 conformer 1	This study	EMDB: EMD-71013
Cryo-EM map of DnaX-complex–β-clamp–1-nt gapped DNA at state 1 conformer 2	This study	EMDB: EMD-71014
Cryo-EM map of DnaX-complex–β-clamp–1-nt gapped DNA at state 1 conformer 3	This study	EMDB: EMD-71015
Cryo-EM map of DnaX-complex–β-clamp–1-nt gapped DNA at state 2 conformer 1	This study	EMDB: EMD-71016
Cryo-EM map of DnaX-complex–β-clamp–1-nt gapped DNA at state 2 conformer 2	This study	EMDB: EMD-71017
Cryo-EM map of DnaX-complex alone	This study	EMDB: EMD-71018
Cryo-EM map of DnaX-complex–β-clamp–10-nt gapped DNA at state 1 DNA recognition	This study	EMDB: EMD-71021
Cryo-EM map of DnaX-complex–β-clamp–10-nt gapped DNA at state 2 conformer 1 fully open_DNA unsettled	This study	EMDB: EMD-71022

Cryo-EM map of DnaX-complex–β-clamp–10-nt gapped DNA at state 2 conformer 2 fully open_DNA settled	This study	EMDB: EMD-71023
Cryo-EM map of DnaX-complex–β-clamp–10-nt gapped DNA at state 2 conformer 3 partially closed	This study	EMDB: EMD-71024
Cryo-EM map of DnaX-complex–β-clamp–10-nt gapped DNA at state 2 conformer 4 fully closed_1	This study	EMDB: EMD-71025
Cryo-EM map of DnaX-complex–β-clamp–10-nt gapped DNA at state 2 conformer 5 fully closed_2	This study	EMDB: EMD-71026
Cryo-EM map of DnaX-complex–β-clamp–10-nt gapped DNA at state 2 conformer 6 fully closed_3	This study	EMDB: EMD-71027
Atomic model of DnaX-complex–β-clamp–1-nt gapped DNA at state 1 conformer 1	This study	PDB: 9OYB
Atomic model of DnaX-complex–β-clamp–1-nt gapped DNA at state 1 conformer 2	This study	PDB: 9OYC
Atomic model of DnaX-complex–β-clamp–1-nt gapped DNA at state 1 conformer 3	This study	PDB: 9OYD
Atomic model of DnaX-complex–β-clamp–1-nt gapped DNA at state 2 conformer 1	This study	PDB: 9OYE
Atomic model of DnaX-complex–β-clamp–1-nt gapped DNA at state 2 conformer 2	This study	PDB: 9OYF
Atomic model of DnaX-complex alone	This study	PDB: 9OYG
Atomic model of DnaX-complex–β-clamp–10-nt gapped DNA at state 1 DNA recognition	This study	PDB: 9OYH
Atomic model of DnaX-complex–β-clamp–10-nt gapped DNA at state 2 conformer 1 fully open_DNA unsettled	This study	PDB: 9OYI
Atomic model of DnaX-complex–β-clamp–10-nt gapped DNA at state 2 conformer 2 fully open_DNA settled	This study	PDB: 9OYJ

Atomic model of DnaX-complex–β-clamp–10-nt gapped DNA at state 2 conformer 3 partially closed	This study	PDB: 9OYK
Atomic model of DnaX-complex–β-clamp–10-nt gapped DNA at state 2 conformer 4 fully closed_1	This study	PDB: 9OYL
Atomic model of DnaX-complex–β-clamp–10-nt gapped DNA at state 2 conformer 5 fully closed_2	This study	PDB: 9OYM
Atomic model of DnaX-complex–β-clamp–10-nt gapped DNA at state 2 conformer 6 fully closed_3	This study	PDB: 9OYN
Oligonucleotides		
gBlocks HiFi gene fragments	Integrated DNA Technologies	N/A
5′- GGCTCGCTACGGCTATACGG/Cy3/ -3′ (Primer 1 for 1-nt and 10-nt gapped DNA in cryo-EM, also for binding affinity assay)	Integrated DNA Technologies	N/A
5′- GATTCGTATCGCCTATACCG -3′ (Primer 2 for 1-nt and 10-nt gapped DNA in cryo-EM, also for binding affinity assay)	Integrated DNA Technologies	N/A
5′- CGGTATAGGCGATACGAATCTCCGTA TAGCCGTAGCGAGCC -3′ (Tmpl_41-nt for 1-nt gapped DNA in cryo-EM)	Integrated DNA Technologies	N/A
5′- CGGTATAGGCGATACGAATC$(T)_{10}$CCGTA TAGCCGTAGCGAGCC -3′ (Tmpl_50-nt for 10-nt gapped DNA in cryo-EM, also for binding affinity assay)	Integrated DNA Technologies	N/A
5′- CGGTATAGGCGATACGAATC$(T)_{30}$CCGTA TAGCCGTAGCGAGCC -3′ (Tmpl_70-nt for binding affinity assay)	Integrated DNA Technologies	N/A
5′- BioTEG/GGGAAGGGCGATCGGTGCGGG CCTCTTCGCTATTACGCCAGCTGGCGAAA GGGGGATGTGCTGCAAGGCGATTAAGTTG GGTAACGC -3′ (M13 primer)	Integrated DNA Technologies	N/A

5′- BioTEG/CTGGATGAGTTGAGTGGACGGC TGCAGCAAGTCACCAATGTCTAAGAGTTC GTATTATGCCTACACTGGAGTACCGGAGCA TCGTCGTGACTGGGAAACT/BioTEG/ -3′ (replication template)	Integrated DNA Technologies	N/A
5′- AGTTTCCCAGTCACGACGATGCTCCGG TAC -3′ (replication primer 1)	Integrated DNA Technologies	N/A
5′- GCAGCCGTCCACTCAACTCATCCAG -3′ (replication primer 2)	Integrated DNA Technologies	N/A
Recombinant DNA		
cAMP-dependent protein kinase	Kelman et al.,[62] 1995	Sigma # P2645
DnaX-complex expression plasmids	Onrust et al.,[63] 1995	Addgene numbers for expression of the five subunits: (E coli DnaX tau only, 237237; Ec holA pET11a, 237233; Ec holB pET11a, 237234; Ec holC pET 3c, 237235; Ec hold pET 3c, 237236)
Pol III αε expression plasmids	Studwell et al.,[64] 1990	Addgene
SSB expression plasmid	Studwell et al.,[64] 1990	Addgene # 237240
β-clamp expression plasmid	Studwell et al.,[64] 1990	Addgene # 237238
Kinase tagged β-clamp expression plasmid	Kelman et al 1994, PMID: 8594367	Addgene # 237239
Software and algorithms		
SerialEM	Mastronarde,[65] 2003	https://bio3d.colorado.edu/SerialEM/
cryoSPARC v4.3.1 and v4.5.3	Punjani et al.,[66] 2017	https://cryosparc.com/
Relion 5.0	Scheres,[67] 2012	https://relion.readthedocs.io/en/release-5.0/
MotionCor2	Zheng et al.,[68] 2017	https://emcore.ucsf.edu/ucsf-software

CTFFIND4	Rohou and Grigorieff,[69] 2015	https://grigoriefflab.janelia.org/ctffind4
Topaz	Bepler et al.,[70] 2019	https://cb.csail.mit.edu/cb/topaz/
PyEM	Asarnow et al.,[71] 2019	https://zenodo.org/record/3576630#.ZDbbk-zMLsc
UCSF Chimera	Pettersen et al.,[72] 2004	http://www.cgl.ucsf.edu/chimera/
UCSF Chimera X	Goddard et al.,[73] 2018	https://www.cgl.ucsf.edu/chimerax/
Coot	Emsley et al.,[74] 2010	http://www2.mrc-lmb.cam.ac.uk/personal/pemsley/coot
PHENIX	Adams et al.,[75] 2010	https://phenix-online.org
Other		
Quantifoil Au R1.2/1.3 300 mesh grids	SPI Supplies	Cat# 4230G-XA
Quantifoil UltrAu R1.2/1.3 300 mesh grids	SPI Supplies	Cat# 4976G-FA
Gatan Solarus plasma cleaner 950	Gatan	N/A
Vitrobot Mark IV	Thermo Fisher Scientific	N/A
Talos Arctica Cryo-TEM	Thermo Fisher Scientific	N/A
Titan Krios G2 Cryo-TEM	Thermo Fisher Scientific	N/A

RESOURCE AVAILABILITY

Lead contact. Further information and requests for reagents and resources may be directed to, and will be fulfilled by the Lead Contact Huilin Li (Huilin.Li@vai.org)

Materials availability. All plasmid clones used to express the proteins used in this study are available upon request without restrictions, although an MTA may be required.

Data and code availability

380 • Five conformers of DnaX-complex with β-clamp–1-nt gapped DNA in states 1 and 2 have been
381 deposited in the Electron Microscopy Data Bank with accession codes EMD-71013, EMD-71014,
382 EMD-71015, EMD-71016, EMD-71017. Their corresponding atomic models have been deposited in
383 the Protein Data Bank with accession codes 9OYB, 9OYC, 9OYD, 9OYE and 9OYF. These data will
384 be publicly available as of the date of publication.
385 • One DnaX-complex alone, and seven conformers of DnaX-complex-β-clamp–10-nt gapped DNA
386 cryo-EM maps have been deposited in the Electron Microscopy Data Bank with accession codes
387 EMD-71018, EMD-71021, EMD-71022, EMD-71023, EMD-71024, EMD-71025, EMD-71026 and
388 EMD-71027 respectively. Their corresponding atomic models have been deposited in the Protein
389 Data Bank with accession codes 9OYG, 9OYH, 9OYI, 9OYJ, 9OYK, 9OYL, 9OYM and 9OYN. These
390 data will be publicly available as of the date of publication.
391 • This paper does not report original code.
392 • Clones used for expression of factors in this report are deposited in the Addgene repository.
393 • Any additional information required to reanalyze the data reported in this work will be available from
394 the lead contact upon request.
395

396 **EXPERIMENTAL MODEL AND STUDY PARTICIPANT DETAILS**

397 **Bacterial strains**

398 The expression plasmids of *E. coli* DnaX-complexes, i.e., γ-complex ($\delta\gamma_3\delta'\psi\chi$, for biochemical studies)
399 and τ-complex ($\delta\tau_3\delta'\psi\chi$, for cryo-EM studies), β-clamp and their related mutants, SSB, and Pol III αε
400 complex were generated as described[63,64]. Expression of each protein used the expression plasmids
401 listed in the key resources table, transformed into the BL21(DE3) strain of *E. coli* (Thermo Fisher
402 Scientific) and cultured in LB media (**Figure S1**).
403

404 **METHOD DETAILS**

405 **Protein expression and purification**

406 *E. coli* DnaX-complex subunits δ, γ, τ, δ′, ψ and χ were purified as described in[63]. The β, Pol III αε and
407 SSB were purified as described in[64]. The clamp loader γ-complex was reconstituted from pure subunit
408 preparations and purified by ion exchange using a Cytiva MonoQ column as described[63]. Briefly, pure
409 subunit preparations (1–4 mg each in approximately 3 ml of 20 mM Tris-HCl, pH 7.5, 1mM DTT, 0.5 mM
410 EDTA, 10% glycerol) were mixed at a molar ratio of δ: γ_3: δ′: ψ: χ=1.5: 1: 1.5: 1.5: 2. The subunit mixture
411 was incubated for 30 min at 15 °C, then applied to a 1 ml MonoQ column (GE Healthcare, Chicago, IL),
412 followed by elution with a 10 column volume linear gradient of Buffer A (20 mM Tris-HCl pH 7.5, 0.5 mM
413 DTT, 1 mM EDTA, 10% glycerol) plus 50 mM NaCl, collecting 0.2 ml fractions. Fractions were analyzed
414 in a 12% SDS-PAGE. The γ-complex elutes at approximately 0.4 M NaCl, while individual proteins and

415 their subcomplexes elute earlier. The τ-complex was reconstituted and purified in the same way as γ-
416 complex, except that τ was substituted for γ. Peak fractions of each complex were pooled and dialyzed
417 against Buffer A plus 50 mM NaCl, then aliquoted and snap frozen in liquid nitrogen and stored at -80 °C.
418

419 **Mutant β-clamp preparation**

420 gBlocks of HiFi gene fragments were designed to contain the entire *dnaN* gene, including an N-terminal
421 3×FLAG tag followed by a protein kinase A site (LRRASLG)[76]. gBlocks were cloned into pRSFDuet
422 (Novagen, Burlington, MA) that had been digested with NcoI-HF/BamHI-HF and treated with alkaline
423 phosphatase. This procedure was performed for expression of wt and two mutated β-clamps, each
424 having 3 amino acid substitutions ($\beta^{R96A, R103A, R105A}$ and $\beta^{R96E, R103E, R105E}$). gBlocks were dissolved in 20
425 mM Tris-acetate pH 7.9, 50 mM K-OAc, 10 mM $MgCl_2$, 100 µg/ml BSA and digested with NcoI-HF &
426 BamHI-HF. Plasmids were transformed into DH5α cells (ThermoFisher, Waltham, MA) and plated on LB-
427 agar plates containing kanamycin (50 µg/ml) and incubated overnight at 37 °C. Colonies were
428 miniprepped, screened for recombinants by size and by NcoI-HF/BamHI-HF restriction digest in native
429 agarose gels, then maxiprepped followed by confirming the correct sequence over the entire *dnaN* gene
430 by Sanger Sequencing (Genewiz, South Plainfield, NJ). These procedures yielded the two β mutants,
431 $\beta^{R96A, R103A, R105A}$ and $\beta^{R96E, R103E, R105E}$, as well as wt β. These plasmids were transformed into *E. coli*
432 BL21(DE3), and 3 L each of transformed cells were grown to OD_{600} = 0.6, induced upon addition of 2 mM
433 IPTG for 12 h at 15 °C, then collected by centrifugation and resuspended in Buffer A+ 750 mM NaCl and
434 lysed in a Avestin Emulsi Flex-C-50 (Ottawa, ON, Canada). 1mM PMSF was added to the lysate which
435 was then clarified by centrifugation at 12,500 cpm in a F14-6X250 rotor (ThermoFisher, Waltham, MA) at
436 4 ºC for 1 h. Then 5 ml Anti-FLAG beads were added to the clarified supernatant (approximately 400 ml)
437 followed by mixing on an eccentric rocking platform for 30 min at 4 °C. Beads were collected by
438 centrifugation and resuspended in 450 ml Buffer A plus 300 mM NaCl. The Anti-Flag beads were then
439 resuspended in 400 ml Buffer A plus 300 mM NaCl and spun again, and this procedure was repeated
440 two more times. The final bead pellet was resuspended in 15 ml Buffer A plus 50 mM NaCl and loaded
441 onto a XK-16/20 column (Cytiva, Marlborough, MA) whereupon it was further washed using 15 ml Buffer
442 A plus 1M NaCl. The column was then equilibrated to Buffer A plus 50 mM NaCl, and elution was
443 performed in pulses using 5 ml 30 min pulses of Buffer A plus 50 mM NaCl containing 0.23 mg/ml
444 3×FLAG peptide. Elution was performed 4 times and fractions were analyzed by SDS-PAGE. Relevant
445 fractions were pooled, dialyzed against Buffer A, concentrated to approximately 2 mg/ml and stored
446 frozen at -80 °C.
447

448 **Mass photometry**

449 Data were collected using a OneMP mass photometer (Refeyn) that was calibrated with bovine serum
450 albumin (66 kDa), beta amylase (224 kDa), and thyroglobulin (670 kDa). Movies were acquired for 6,000

451 frames (60 s) using AcquireMP software (version 2.4.0) and default settings. Final protein concentrations
452 were empirically determined to achieve ~75 binding events per second. Peak mass values are predicted
453 to fall within ~5% error. Raw data were converted to frequency distributions using Prism 9 (GraphPad)
454 and a bin size of 10 Da.
455
456 **Mutant γ subunit preparation**
457 The δ Y316A mutant was cloned using HiFi DNA encompassing the region of *holA* (gene encoding δ)
458 from the internal AflII site to the BamHI site downstream of the stop codon, including placement of a C-
459 terminal 3×FLAG tag. This gBlock was inserted into the AflII/BamHI digested pET11-holA to yield pET11-
460 holA(Y316A). The full sequence of the mutant *holA* gene was verified by Sanger Sequencing. The
461 pET11-holA(Y316A) plasmid was transformed into Bl21(DE3) *E. coli* cells and 12L of cells were grown
462 under ampicillin selection, induced with 2 mM IPTG, and lysed in a Avestin Emulsi Flex-C-50 (Ottawa,
463 ON, Canada). Purification of δ Y316A was as described above for β mutants, then concentrated and
464 stored frozen at -80 °C. Gamma complex was formed upon mixing the δ Y316A mutant with γ, δ', χ and ψ
465 and purified as described earlier[63], and as briefly described above.
466
467 **Gel filtration-based β-clamp loading assay**
468 Analysis of β loading onto DNA was performed using γ-complex and isotropic ^{32}P labelled β; and the ^{32}P-
469 β-DNA complex was separated from unbound ^{32}P-β by gel filtration through a 5 ml BioGel A15m column
470 essentially as described[77]. Briefly, β was labeled with ^{32}P upon incubating 1 nmol flag-kinase tagged wt β
471 or mutant β using 100 μl of buffer A plus 16.7 pmol γ-^{32}P-ATP, 0.45 μg PKA kinase (Sigma, St Louis,
472 MO) followed by incubation for 30 min at 37°C. ^{32}P-β was purified from unbound ^{32}P-ATP through a
473 Cytiva G25 microspin column equilibrated with buffer A plus 50 mM NaCl. The concentration and specific
474 radioactivity of the purified ^{32}P-β (wildtype β and two mutants) were measured by Bradford assay and by
475 liquid scintillation. The ^{32}P-β was loaded onto either a nicked or 20-nt gapped circular 3 kb plasmid or
476 onto singly-primed M13 ssDNA. The nicked and 20-nt gapped DNAs were constructed from pUC19
477 plasmid DNA as described[78]. The singly-primed DNA was prepared by annealing the biotinylated M13
478 primer (**Table S1**) to M13 ssDNA to which a 5-fold molar excess of streptavidin was added. Reactions
479 contained 1 pmol (10 nM) nicked or gapped plasmid DNA, or primed M13 ssDNA, 2 pmol (20 nM) ^{32}P-
480 FlagPK-β (as dimer) and γ-complex (concentration is noted in the figure legends) in 100 μl of Buffer B
481 (20 mM Tris-HCl, pH7.5, 0.1 mM EDTA, 40 μg/ml BSA, 4% glycerol, 5 mM dithiothreitol) plus 8 mM
482 $MgCl_2$ and 2 mM ATP for 5 minutes at 37 °C. DNA-bound ^{32}P-β was separated from free ^{32}P-β by gel
483 filtration through a 5 ml BioGel A15m column equilibrated with Buffer B plus 8 mM $MgCl_2$ and 100 mM
484 NaCl. Fractions of 180 μl were collected, and 150 μl aliquots were measured for radioactivity via liquid
485 scintillation counting. Radioactivity was converted to fmol using the specific radioactivity of ^{32}P-β (i.e.,

486 determined empirically from the measured radioactivity of a known volume and the protein concentration
487 of that same volume).
488
489 **Cryo-EM grids preparation and data collection**
490 The 1-nt gapped DNA and 10-nt gapped DNA used in cryo-EM studies are shown in **Figures 1D, 3A** and
491 **Table S1**. The *in vitro* assembly of the clamp loading complexes with purified *E. coli* DnaX-complex, β-
492 clamp, and DNA substrates followed our previous reconstitution procedure for the yeast Polδ–PCNA–
493 DNA complex[79]. Briefly, 13.0 µl 1-nt gapped DNA at 7.1 µM or 8.0 µl 10-nt gapped DNA at 11.5 µM were
494 mixed with 1.0 µl β-clamp at 77.6 µM, and incubated at 30 °C for 10 min. The mixtures, along with 1.0 µl
495 10 mM ATPγS and 1.0 µl 100 mM Mg-acetate, were added into 7.1 µl DnaX-complex at 8.4 µM
496 concentration. Finally, ultrapure H_2O was added to bring the final reaction volume to 20 µl. The mixture
497 was incubated in an ice-water bath for an additional 10 min before preparation of cryo-grids.
498
499 The 300 mesh Quantifoil Au or UltrAu R1.2/1.3 grids were glow discharged for 0.5 or 3 min respectively,
500 in a Gatan Solarus, then 3 µl of the loading mixture was applied onto the EM grids. Sample vitrification
501 was performed in a Vitrobot (Thermo Fisher Mark IV) with the following settings: (i) for Au grids, blot time
502 2 s; (ii) for UltrAu grids, blot time 2.5 s; blot force 3 (arbitrary unit), wait time 5 s; inner chamber
503 temperature 6 °C with 95% relative humidity. The EM grids were flash-frozen in liquid ethane cooled by
504 liquid nitrogen. Cryo-EM data were automatically collected in a multi-hole mode on a 300 kV Titian Krios
505 (for 1-nt and 10-nt gapped DNA) controlled by SerialEM[65]. The micrographs were captured at a scope
506 magnification of 105,000× on a K3 direct electron detector (Gatan) operated in the super-resolution video
507 mode with the scope objective lens under-focused in the range of 1.2 to 1.6 µm. For sample with 1-nt
508 gapped DNA, 111-frame movie micrographs were recorded in 3.4 s exposure and with a total dose of
509 49.6 $e^-/Å^2$. For sample with 10-nt gapped DNA, 50-frame movie micrographs were recorded in 1 s
510 exposure with a total dose of 59 $e^-/Å^2$. The calibrated physical pixel size of the K3 detector in Titan Krios
511 was 0.828 Å at the specimen level. See details in **Tables 1** and **S2**.
512
513 **Cryo-EM data processing**
514 Two datasets with 16,140 and 27,515 raw micrographs were recorded for the DnaX-complex–β-clamp
515 with 1-nt gapped DNA or with 10-nt gapped DNA, respectively. Image quality was monitored during data
516 collection by cryoSPARC Live v4.3.1 and v4.5.3[66] installed in a local workstation. The image
517 preprocessing including patch motion correction (bin 2), contrast transfer function (CTF) estimation and
518 correction, blob particle picking (70-150 Å diameter), and particle extraction (bin 4) were also performed
519 at the same time. After two-dimensional (2D) classification, "good" particle images with clear structural
520 features were selected and used to train the picking model in the program Topaz[70] for further particle
521 picking. After 2D cleaning, the selected particles were combined, and duplicate particles with ⩾ 40%

522 overlapping were removed, i.e., only one of two adjacent particles within ⩽ 80 Å distance was kept.
523 (**Figures S2**, **S4**).
524
525 For the dataset with 1-nt gapped DNA **(**16,140 micrographs), the 4.1 million particles after duplicate
526 removal were used for ab initio 3D reconstruction and heterogeneous refinement with 4 3D classes.
527 Besides two junk volumes, we obtained two major states of the DnaX-complex–β-clamp–1-nt gapped
528 DNA, referred to here as states 1 and 2, with 1.8 and 1.7 million particles respectively. The first state
529 represents an initial DNA recognition state, and the second state has the 3′-dsDNA inside the β-clamp
530 with the DNA gate being closed to a variable extent, but with the 5′-dsDNA unexpectedly bending sharply
531 back towards the 3′-dsDNA bound to the outer surface of the β-clamp (**Figure S2**). After non-uniform
532 refinement, the maps and associated particle images were transferred into RELION 5.0.0 for further 3D
533 classification without alignment, followed by focused 3D classification on DNA as marked by the red
534 dashed oval shape. Then, the selected classes were transferred back to cryoSPARC v4.5.3 for global
535 and local CTF refinement to fix the aberrations introduced by UltrAu grid, followed by reference-based
536 motion correction, and non-uniform and local refinement.
537
538 We finally obtained three conformers belonging to the first major state: conformer 1 at 3.14 Å resolution
539 with 105,100 particles and of 6% population, in which 9 bp of the 20-bp 5-dsDNA was visualized at the
540 loader shoulder; conformer 2 at 2.71 Å resolution with 228,387 particles and with 5 bp of the 5′-dsDNA
541 visualized; and conformer 3 at 2.73 Å resolution with 232,057 particles and with a fully disordered 5′-
542 dsDNA (**Figures S2**–**3**). We obtained two conformers belonging to the second major state: conformer 1
543 at 2.72 Å resolution with 283,092 particles in which the 3′-dsDNA has entered the β-clamp, and the 5′-
544 dsDNA bends down and binds to the basic patch on the fully open β-clamp; conformer 2 at 3.12 Å
545 resolution with 203,554 particles in which the 3′-dsDNA has entered a bit further, the 5′-dsDNA has
546 dissociated from β-clamp, and the β-clamp gate is narrowed by 7 Å relative to conformer 1 (**Figures 2**
547 and **S2**–**3**). Following the emerging trend of using the machine-learning derived tools to improve EM map
548 visualization and interpretation[80,81], we applied EMReady v2.2.1 to the 3D EM maps of all five conformers
549 described above.
550
551 For the dataset with 10-nt gapped DNA (27,515 micrographs), a total of ~8.5 million particles were used
552 to generate three initial maps by ab initio 3D reconstruction, followed by heterogeneous refinement with 3
553 classes in cryoSPARC. The first 3D class had no structural feature and was discarded. The second class
554 with ~ 3.1 million particles was from DnaX-complex alone (without β-clamp and DNA). This class was
555 selected for two more rounds of 2D classification, and the selected particles were subjected to
556 heterogeneous refinement with 3 copies of initial map as references. One resulting 3D class with

557 478,123 particles and the best structural features was selected for further reference-based motion
558 correction and non-uniform refinement, leading to a final map at 2.95 Å resolution (**Figures S4**–**5**). The
559 third 3D class with ~ 4.7 million particles was from the ternary DnaX-complex–β-clamp–10-nt gapped
560 DNA complex. This class was subjected to another round of heterogeneous refinement using 8 copies of
561 the initial map as references. Among the resulting 8 classes, 4 were discarded due to lacking structural
562 features and low resolution (4 Å to 7 Å). The remaining four had higher resolutions (3.38 Å to 3.57 Å): #1
563 is a novel state in which the 3′-dsDNA has entered the loader chamber but its blunt end remains outside
564 the β-clamp (termed as DNA recognition); #2 has the 3′-dsDNA inside the chambers of both DnaX-
565 complex and β-clamp but the β-clamp remains fully open; #3-4 has the β-clamp gate fully closed but has
566 some variable flexibility in β-clamp.
567
568 After further 3D classification, combination of similar classes, reference-based motion correction and
569 non-uniform refinement, we obtained 7 conformers of the DnaX-complex–β-clamp–10-nt gapped DNA:
570 #1 with 473,295 particles at 2.54 Å resolution in the DNA recognition state; #2 with 502,506 particles at
571 2.54 Å resolution has the β-clamp gate fully open, but the 3′-dsDNA has not reached the center of the β-
572 clamp (fully open_DNA unsettled); #3 with 499,551 particles at 2.53 Å resolution has the β-clamp gate
573 fully open and the 3′-dsDNA near the center of the β-clamp (fully open_DNA settled); #4 with 476,182
574 particles at 2.60 Å resolution has the β-clamp gate partially closed state; #5–7 with 360,948, 539,340,
575 443,597 particles and at 2.88, 2.60 and 2.70 Å resolution, respectively, have their β-clamp gates fully
576 closed but the interfaces between DnaX-complex and β-clamp vary among the three (**Figures S4**–**5**).
577
578 The clamp loader we used in cryo-EM analysis was the DnaX-holo-complex containing both ψ and χ
579 subunits. ψ and χ are quite small, with 137 and 147 aa at 15.2 and 16.6 kDa, respectively. We observed
580 a fuzzy density at the expected ψχ binding site on the loader in some 2D class averages. Thus we
581 combined all ψ–χ containing particles (~ 7.8 million) after heterogeneous refinement including the loader
582 alone and loader bound to clamp and 10-nt gapped DNA, converted these particles by PyEM[82] to
583 RELION 5.0.0[83]. We generated a focused mask around the ψχ density, then performed three rounds of
584 focused 3D classification into 8 classes without alignment. One class with 242,505 particles at 7.10 Å
585 resolution had good density features was selected and converted back to cryoSPARC for local
586 refinement, leading to an improved map of the 32-kDa heterodimer at 5.50 Å resolution (**Figure S4**).
587 Then, we merged this local map with the 3D map of the DNA recognition state to generate a composite
588 map, which represents the ψχ containing DnaX-holo-complex loading β-clamp onto the 10-nt gapped
589 DNA.
590
591 **Model building, refinement, and validation**

592 The crystal structures of the γ-complex (PDB 1JR3)[7], β-clamp–DNA (PDB 3BEP)[84] and SSB peptide
593 bound ψ–χ subcomplex (PDB 3SXU)[32] were fitted into the composite cryo-EM map of DnaX-holo-
594 complex bound to β-clamp and 10-nt gapped DNA at the first state (DNA recognition). The docked
595 structures were merged into one using ChimeraX[73] and served as the starting model. The automated *de*
596 *novo* modeling program ModelAngelo was also used to facilitate model building[85]. After manual
597 refinement in COOT[74], the resulting model was fed into PHENIX[75] for real space refinement, followed by
598 two rounds of iterative refinement between PHENIX and COOT. Then, ISOLDE, a molecular-dynamics
599 flexible fitting-based plugin of ChimeraX, was used to minimize model clashes. The final model was
600 validated by the MolProbity program embedded in PHENIX[86]. This model then served as the initial model
601 for modeling the 3D EM maps of the five loading conformers with 1-nt gapped DNA and the 3D EM maps
602 of the seven loading conformers with 10-nt gapped DNA. In the regions with weak densities, such as
603 near the open gate of the β-clamp, the model was rigid body docked, followed by manual adjustment in
604 COOT and finally refined in real space in PHENIX. Refinement of all models followed the same
605 procedure. The statistics of model refinement and validation are listed in **Tables 1 and S2**. Structural
606 panels were prepared in ChimeraX[87] and assembled into figures in Adobe Illustrator (Adobe Inc, San
607 Jose, CA).
608
609 **Fluorescence polarization-based DNA binding assay**
610 The affinity of γ-complex binding to DNA was measured using either a tailed DNA (primer/template, p/T)
611 or a 10- or a 30-nt gapped DNA at a constant DNA concentration of 10 nM. The DNA oligos were gel
612 purified. The DNA substrates were made by annealing 3′ Cy3-labelled Primer 1 either with a 50-nt
613 template (template), or with Primer 2 and 50-nt template, or with Primer 2 and 70-nt template (**Figure 5B,**
614 **Table S1**), followed by purification on a 10% native-PAGE. Gel bands were cut out, and the DNA
615 substrates were extracted in TE buffer (10 mM Tris-HCl pH 7.5, 1 mM EDTA) and further concentrated
616 and buffer exchanged into TE.
617
618 Fluorescence polarization-based DNA binding experiments were performed by titrating γ-complex from 0
619 to 600 nM into reactions at 50 μL final volume containing 20 mM Tris-HCl (pH 7.5), 40 mM NaCl, 8
620 mM $MgCl_2$, 1 mM TCEP, 0.1 mM EDTA and 100 μM ATPγS. The reaction mixtures were performed in a
621 384-well plate, then incubated at 23 °C for 20 min. The plates were centrifuged for 20 sec to eliminate
622 any bubbles, and the fluorescence intensity was recorded using a Synergy Neo2 plate reader fluorimeter
623 (Agilent, Sant Clara, CA) by exciting the Cy3 fluorophore at 535 nm and reading the integrated
624 fluorescence emission signal between 560-580 nm. Three independent experiments were performed for
625 each titration. Relative intensity (I/I_0) was plotted versus γ-complex concentration. Apparent K_d ($^{App}K_d$)
626 measurements were determined using a one-site binding model using the Origin Software (OriginLab,
627 Northampton, MA).

628

629 **Measurement of clamp loading rate onto primed versus gapped DNA**

630 Rate of clamp loading was determined by a replication assay using Pol III$\alpha\varepsilon$ complex, which requires the
631 loaded β-clamp to extend a primed site (**Figures 5C** and **S7**). Therefore, β-clamp was loaded onto a 5′
632 ^{32}P-primed site in the presence of γ-complex and Pol III$\alpha\varepsilon$ complex, and timed aliquots were removed for
633 analysis in a urea-PAGE. To make clamp loading the rate-limiting step, we used Pol III in sufficient
634 amount to ensure that the distribution of reaction products depended on clamp loading but not on the Pol
635 III rate of primer extension. Specifically, under conditions in which clamp loading is rate limiting, DNA
636 products at all time points should have the same distribution in a urea-PAGE but should become more
637 intense with time. We also performed a control containing only Pol III (lacking β-clamp and γ-complex);
638 and the result showed no primer extension as expected. The DNA template (replication template) and
639 the 5′ ^{32}P-primed site (replication primer 1) used in these assays are given in **Table S1**. For the gapped
640 DNA, a second oligonucleotide (replication primer 2) was annealed to the 45-nt template downstream of
641 the 3′ terminus of the 5′ ^{32}P-replication primer 1. The replication template strand contained biotin at both
642 termini to retain loaded clamps. For the singly-primed DNA, ^{32}P-replication primer 1 was labeled using T4
643 polynucleotide kinase (Sigma, St. Louis, MO) and then annealed to the replication template. For the 45-
644 nt gapped template, both the ^{32}P-replication primer 1 and the unlabeled replication primer 2 were
645 annealed to the replication template. Reactions were assembled in a scaled-up volume of 4.5x reactions
646 (90 μL) such that four 20 μL timed aliquots could be removed and quenched for analysis in a urea-
647 PAGE. Each "scaled up reaction" contained 0.9 pmol ^{32}P-primed template, 5.3 pmol streptavidin tetramer
648 in Buffer B plus 8 mM $MgCl_2$. Reactions were incubated at 23 ºC for 15 min, then 2.7 pmol SSB was
649 added and incubated a further 5 min at 37 °C. Reactions were initiated upon adding 0.9 pmol *E. coli* Pol
650 III, 0.9 pmol β-clamp, 0.9 pmol γ-complex or 0.9 pmol τ-complex in a total of 90 μL buffer B containing 8
651 mM $MgCl_2$, 2 mM ATP and 100 mM dATP, dCTP, dGTP & ^{32}P-dTTP. The mix was incubated at 23 ºC,
652 and 20 μL aliquots were removed after 0.5, 1, 2 and 5 min and quenched with 25 μL stop solution
653 containing 76% formamide, 14 mM EDTA, 0.02% bromophenol blue, and 2% SDS. Replicated products
654 were separated on a 15% urea-denaturing polyacrylamide gel (**Figure S7**). The gel was exposed to a
655 storage phosphor screen, then scanned with a Typhoon phosphorimager (GE Healthcare). Quantification
656 of the products in each lane was performed using ImageQuant software (GE Healthcare). Each reaction
657 was performed in triplicate and the mean and standard deviations were calculated using Microsoft Excel.

658

659 **QUANTIFICATION AND STATISTICAL ANALYSIS**

660 The fluorecence polarization-based binding assays for γ-complex with different DNA substrates were
661 carried out by three independently performed experiments. The data points fitting was performed in
662 Origin Software (OriginLab, Northampton, MA), and shown as mean (SEM) ± standard error (SD) in

663 **Figure 5B**. Statistical analysis of built cryo-EM structures was achieved during refinement in Phenix, see
664 details in **Tables 1** and **S2**.
665
666 **Supplemental video legends**
667 **Video 1. An overview of thirteen β-clamp loading intermediates by DnaX-complex onto either a 1-**
668 **nt gapped DNA (five intermediates) or a 10-nt gapped DNA (eight intermediates).** Related to
669 **Figures 1**–**4**. The thirteen atomic models are rotated 360º around the Y axis. The models are aligned
670 and shown separately.
671
672 **Video 2. Morphing of the β-clamp loading onto the 1-nt gapped DNA.** Related to **Figures 1**–**2**. The
673 morph combines the recent structural information of DnaX-complex loading β-clamp onto tailed DNA[16,17]
674 and the five new loading intermediate structures onto a 1-nt gapped DNA. The video starts with the
675 assembly of a binary complex of DnaX-complex and β-clamp in the presence of ATP. The binding event
676 triggers β-clamp opening. Then, the binary complex binds to the 3′-dsDNA segment of the 1-nt gapped
677 DNA via a basic patch on the outer surface of the β-clamp near the open gate. This is followed by the 5′-
678 dsDNA bending sharply down towards the 3′-dsDNA on the β-clamp, leading to the formation of a
679 stressed U-shaped DNA structure and exposure of the 3′-recessed end. Next, the stress in the DNA
680 drives the exposed DNA 3′-recessed end into the DnaX-complex, the 3′-dsDNA into the β-clamp, and the
681 5′-dsDNA binding to the clamp basic patch just vacated by the 3′-dsDNA. During this process, the δ
682 Y316 sensor recognizes but does not unwind the DNA 3'-recessed end. It is believed that the DNA inside
683 the β-chamber induces gate closure via electrostatic attraction and stimulates ATP hydrolysis, leading to
684 the separation of DnaX-complex from β-clamp, thereby completing the bacterial clamp loading process.
685
686 **Video 3. Morphing of β-clamp loading onto larger gapped DNA (> 6-nt).** Related to **Figures 3**–**4**.
687 This video was made in ChimeraX based on the reported structures of β-clamp (PDB 1MMI)[88] and *E. coli*
688 DnaX-complex bound to β-clamp without DNA (PDB 8GIY, 7TI8)[16,17] and the eight structures captured
689 here with a 10-nt gapped DNA. In the presence of ATP, the *E. coli* clamp loader DnaX-complex binds
690 and opens the gate of the β-clamp. Because it is exposed in a large gapped DNA, the DNA 3′-recessed
691 end can directly enter the loader chamber without obstruction and interacts with the sensor pin δ Y316,
692 while the 3′-dsDNA binds to the basic patch on the exterior of β-clamp. Next, the highly positively
693 charged inner chamber of the β-clamp likely attracts the 3-dsDNA to enter the β-clamp. The same
694 electrostatic attraction between DNA and the clamp inner chamber will also drive the β-clamp gate
695 closure, leading to eventual separation of DnaX-complex from the DNA-encircling β-clamp.

Figures and legends

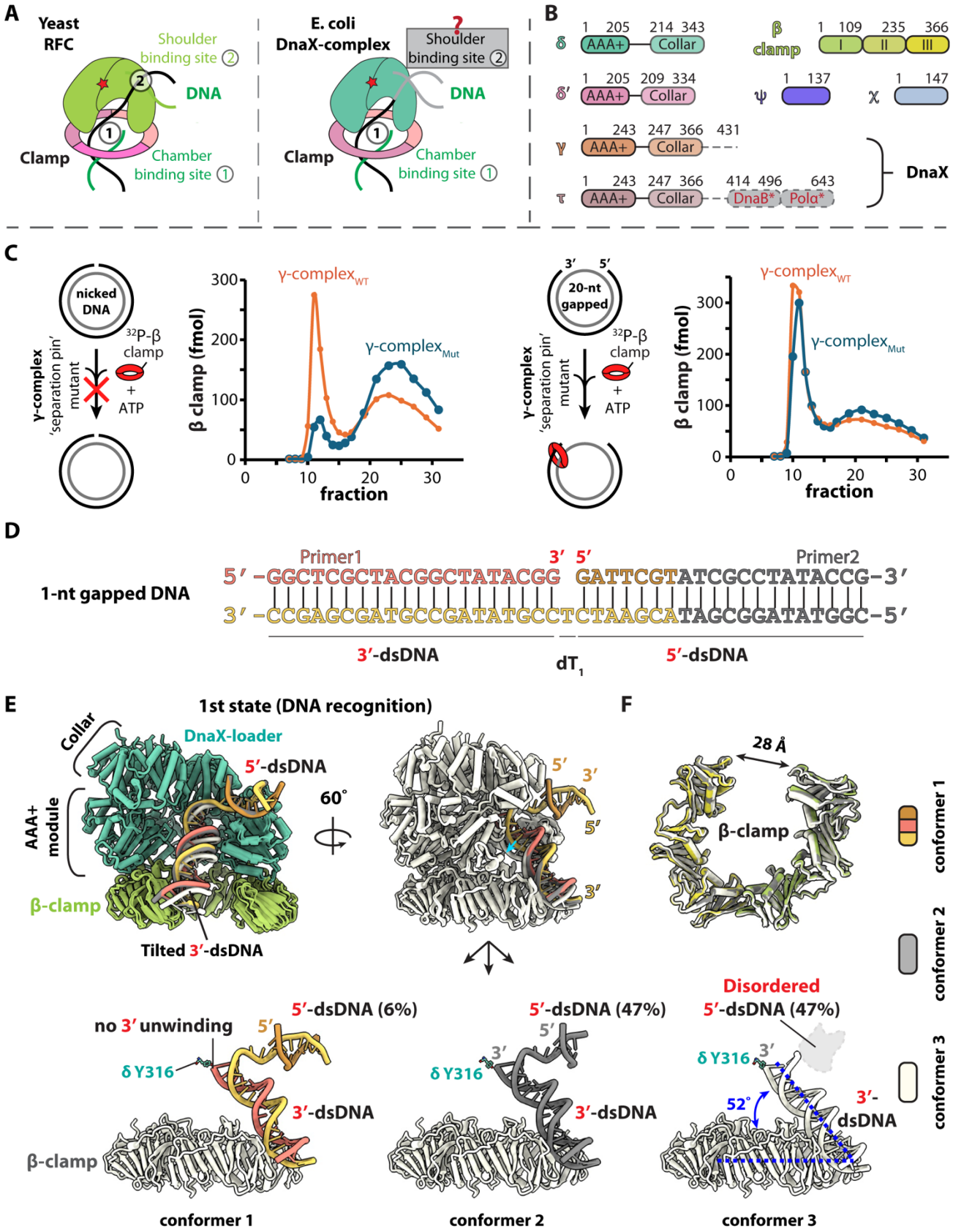

Figure 1. The *E. coli* DnaX-complex loading β-clamp onto a nick or 1-nt gapped DNA. (**A**) Sketch showing that RFC uses a shoulder DNA binding site to facilitate PCNA loading onto small-gaped DNA.

700 How DnaX-complex loads β-clamp to nicks or small gaps and if DnaX-complex harbors a shoulder site
701 are unclear. (**B**) Architecture of the DnaX-holo-complex and the β-clamp subunit. The *E. coli dnaX*
702 encodes the full-length τ and C-terminally truncated γ (missing CTD). The mobile τ CTD (grey) includes
703 regions for DnaB and Pol α binding (asterisks). (**C**) The β-clamp loading assay result by WT and the
704 δ Y316A mutant γ-complex onto a nicked (left) or a 20-nt gapped circular DNA (right). (**D**) Sequence of
705 the 1-nt gapped DNA used in cryo-EM study. The unresolved region is in grey. The dsDNA segment
706 containing the 3′-recessed end is termed 3′-dsDNA, and the dsDNA containing the 5′-recessed end of
707 the 5′-dsDNA. (**E**) Three conformers of the first major loading state – the DNA recognition state – of the
708 DnaX-complex–β-clamp with 1-nt gapped DNA. The top two panels are two views of the three
709 superimposed conformers. In all conformers, the DNA 3′-recessed end has entered the loader chamber,
710 but the 3′-dsDNA is outside the β-clamp. The 5′-dsDNA is only partially ordered in conformer 1 (7 bp) and
711 conformer 2 (5 bp) and totally disordered in conformer 3 (lower panels). Note that no base pair is
712 separated from DNA 3′-recessed end by the δ Y316 as shown in the lower left panel. (**F**) Superimposition
713 of the β-clamps in the three conformers shows the same 28 Å opening. Unless otherwise noted, distance
714 measurements were done in surface view in ChimeraX[73].
715

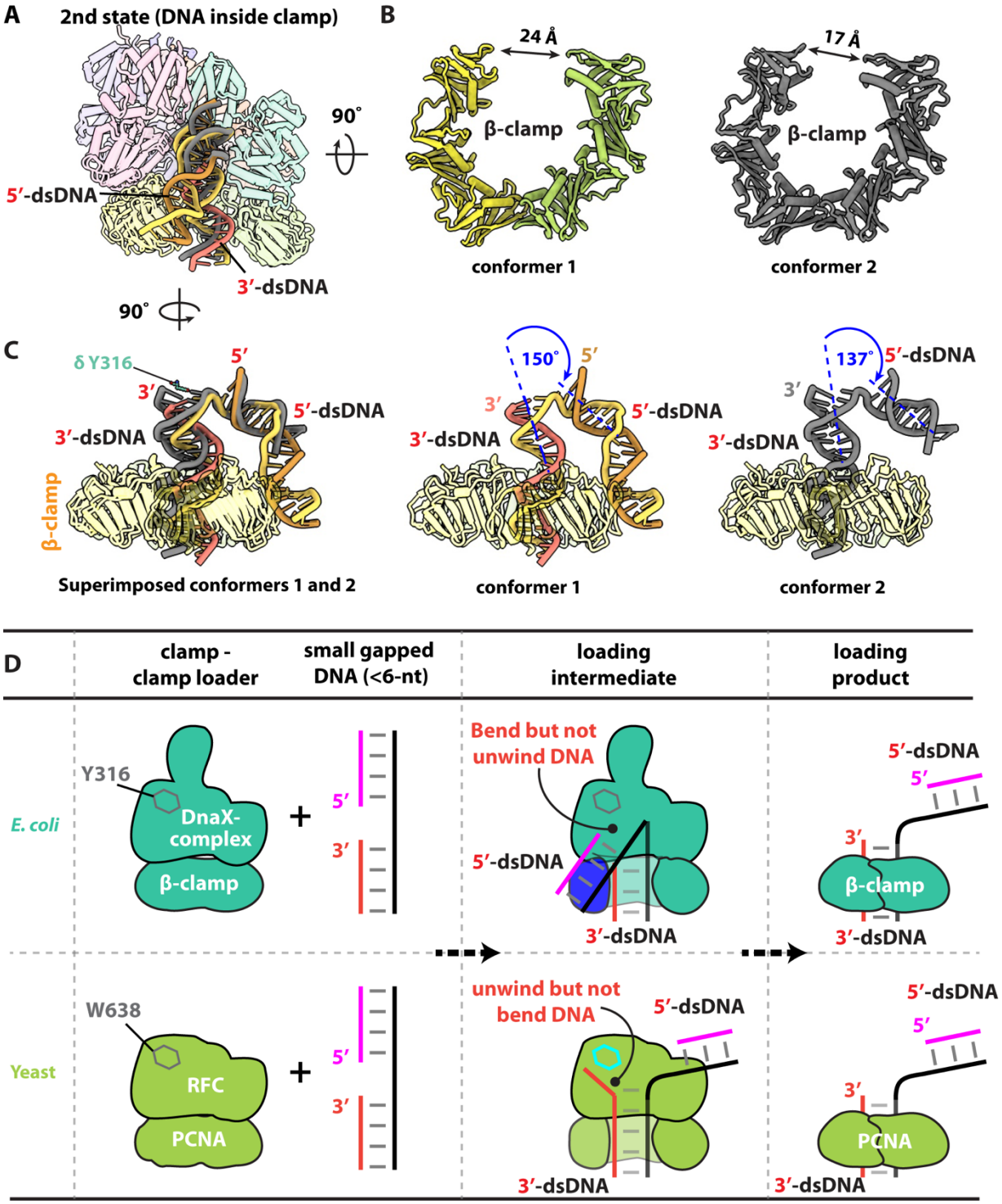

Figure 2. The second state of DnaX-complex loading β-clamp onto 1-nt gapped DNA. (**A**) Superimposition of conformers 1 (color) and 2 (gray) in the second major loading state in which the 3′-dsDNA has entered the clamp chamber. The proteins are shown in 80% transparent cartoons for clarity. (**B**) Side-by-side comparison of the β-clamp in conformers 1 and 2. (**C**) Left side view of (A) but omitting DnaX-complex. The two conformers are shown separately to the right. The 5′-dsDNA binds the outer surface of β-clamp just vacated by the 3′-dsDNA in conformer 1 but dissociates from β-clamp and becomes partially flexible in conformer 2 (only 11 bp). No base pair separation from the 3′-recessed end

occurred. (**D**) Comparison of clamp loading in bacteria (e.g., *E. coli*) and eukaryotes (e.g., *S. cerevisiae*) onto nicks or small gapped DNA. In yeast, the Rfc1 W638 melts up to 6 bp to create a long enough gap for PCNA loading[14,15]. In *E. coli*, the equivalent residue δ Y316 recognizes DNA 3′-end but does not unwind DNA. DnaX-complex, but not RFC, bends DNA by 150° for clamp loading.

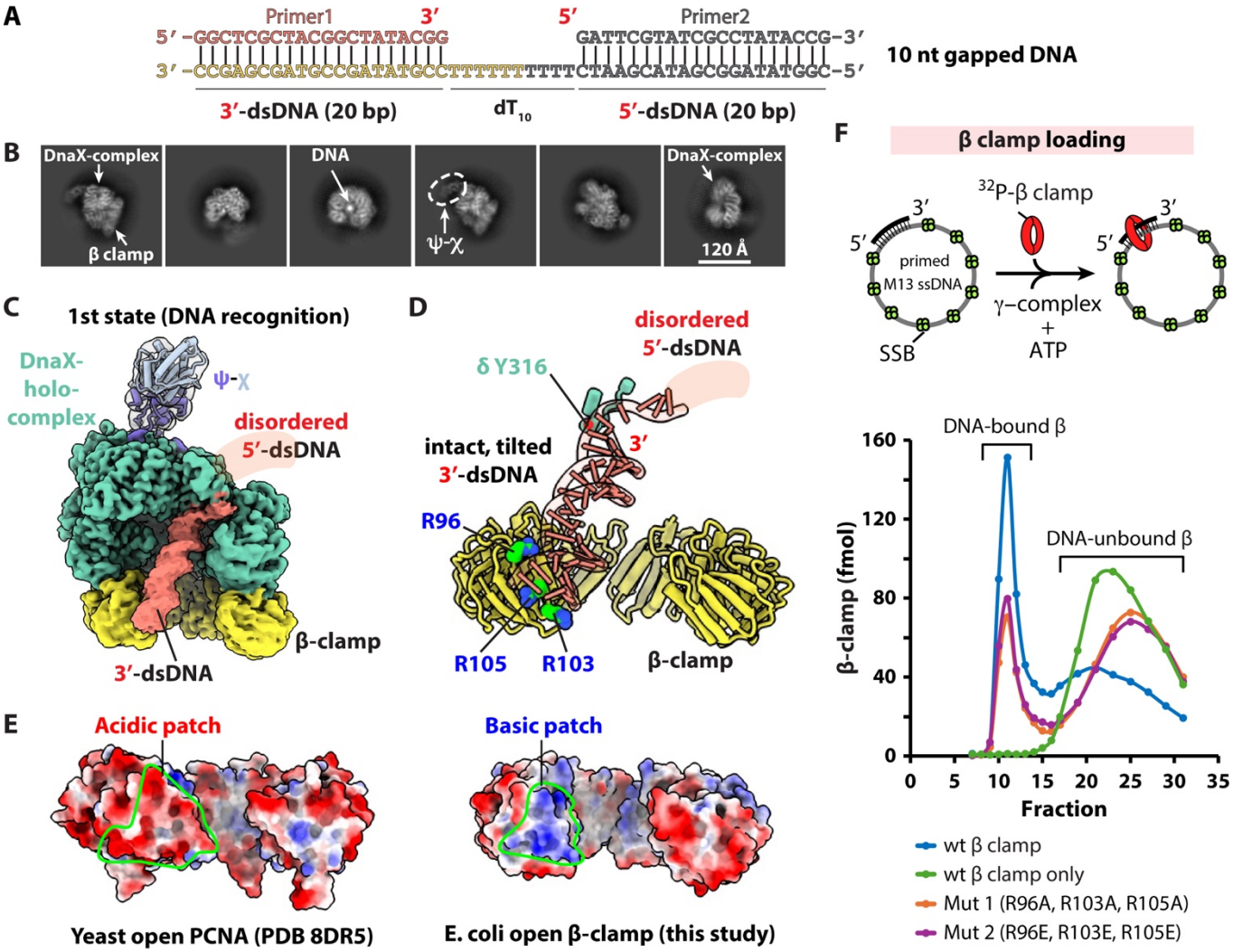

Figure 3. β-clamp loading by DnaX-holo-complex onto a 10-nt gapped DNA. (**A**) Architecture of the 10-nt gapped DNA used in the cryo-EM studies. (**B**) Selected 2D class averages of the loading intermediates. The dashed oval marks the weak density of the ψχ dimer. (**C**) Front view of the DnaX-holo-complex in the first state (DNA recognition state) of loading the clamp onto the 10-nt gapped DNA, with disordered 5′-dsDNA and with the 3′-dsDNA being outside the clamp. (**D**) The blunt end of the 3′-dsDNA binds to the basic patch outside the β-clamp. The three positively charged residues (R96, R103, R105) are shown in spheres. The δ Y316 interacts with but does not unwind from the 3′-recessed end. (**E**) Comparison of the electrostatic potential surface of β-clamp and PCNA. The corresponding basic patch of β-clamp is acidic in PCNA. (**F**) Loading of the basic patch mutant clamps is half as efficient as the WT clamp. The β-clamp is ^{32}P-labelled for quantification.

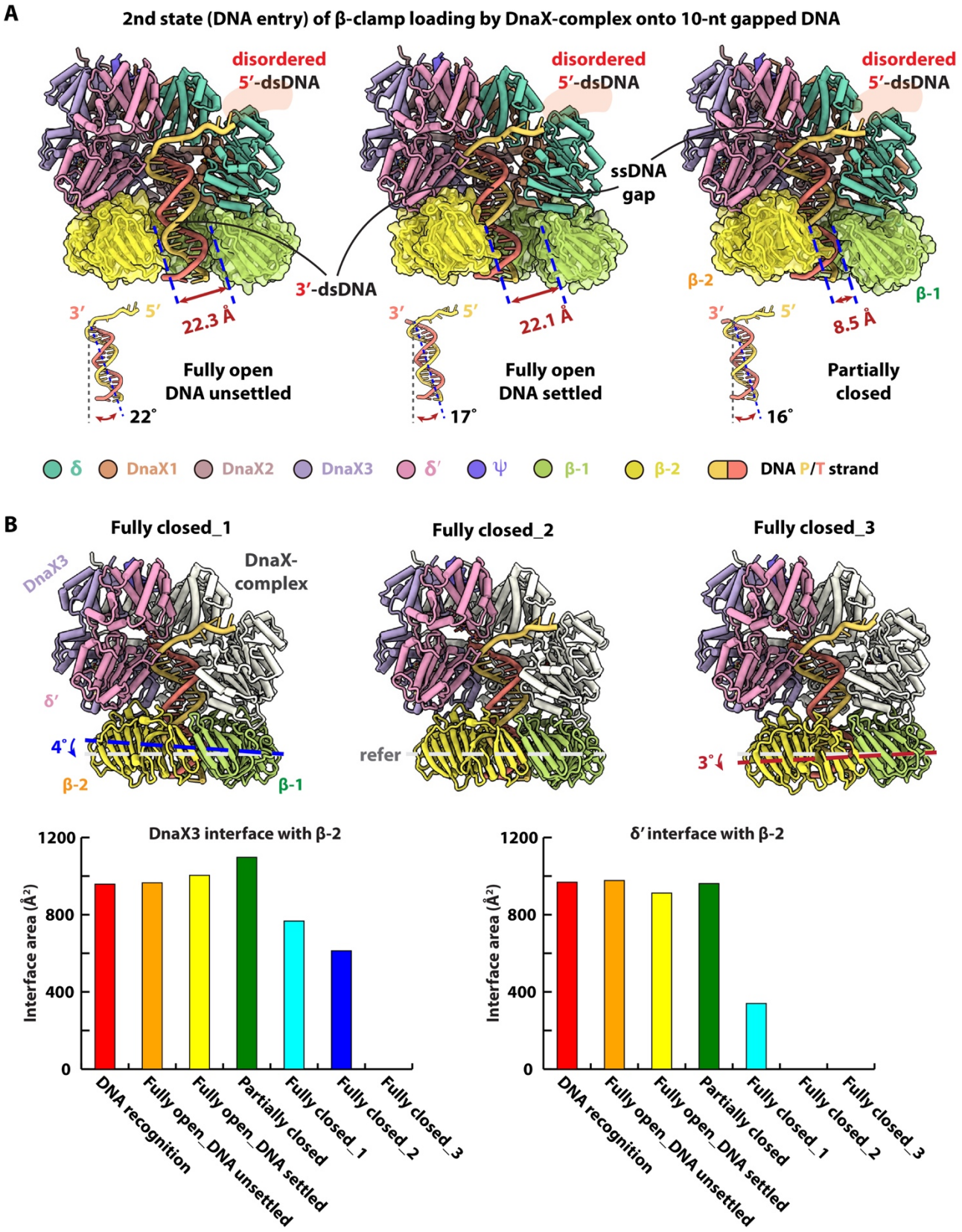

Figure 4. The six conformers in the second state of DnaX-complex loading clamp onto the 10-nt gapped DNA. (**A**) In conformers 1–3, as the 3′-dsDNA gradually settles inside the β-clamp by reducing tilt from 22° to 17° to 16°, the clamp gate gradually closes from 22.3 Å to 22.1 Å to 8.5 Å. (**B**) In the

clamp gate fully closed conformers 4 to 6, β-clamp gradually dissociates from the clamp loader, by the clamp gradually tilting away from the loader by 4° and 3°, respectively. In the lower panels are plotted interface areas between DnaX3 and β-2 subunit (left) and between δ′ and β-2 subunit (right).

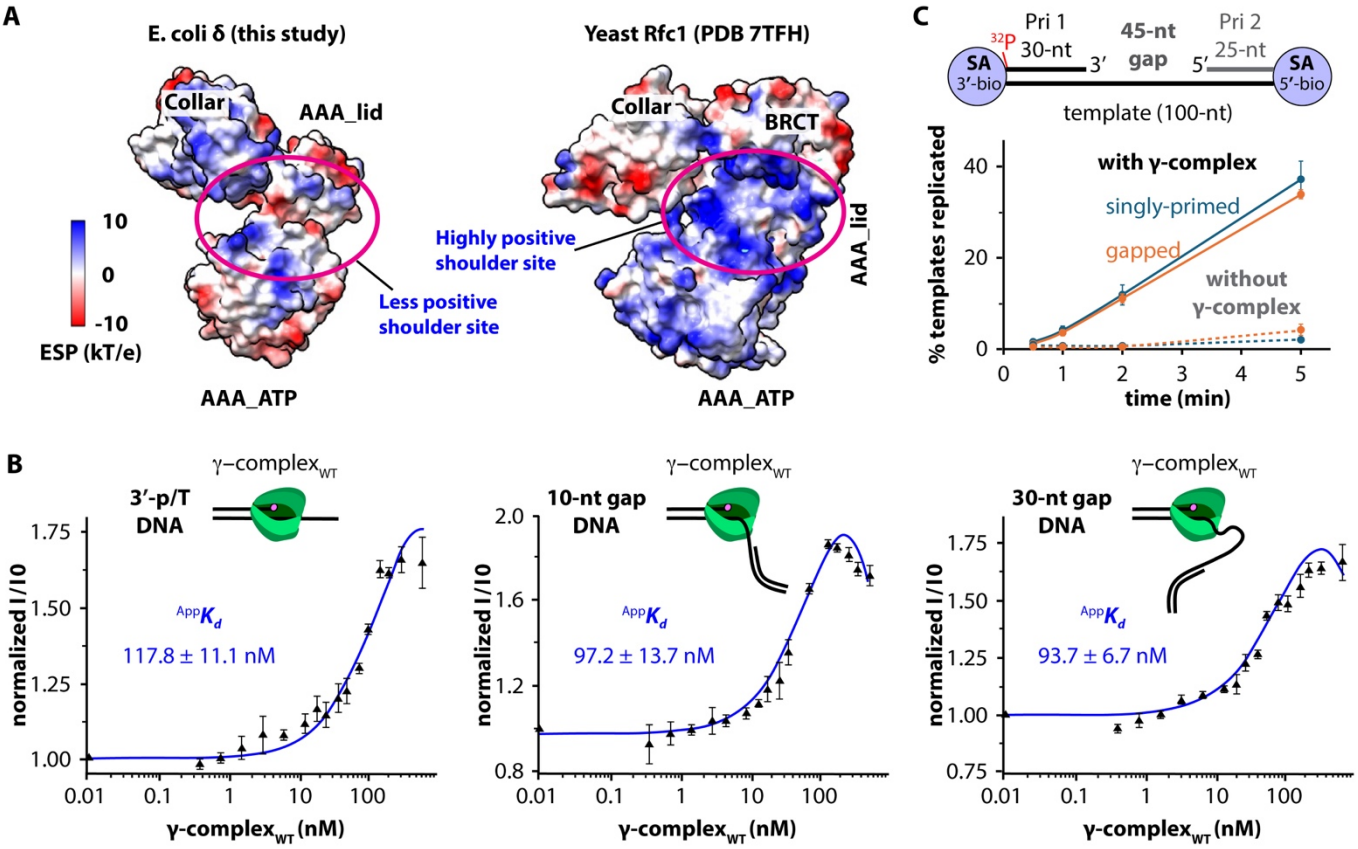

Figure 5. The DnaX-complex shoulder is not highly positively charged and is not essential for clamp loading. (**A**) Comparison of the electrostatic surfaces shows that Rfc1 (PDB: 7TFH) contains a highly positively charged dsDNA binding site (purple oval), while *E. coli* δ (this study) does not contain a similarly charged site. (**B**) The fluorescence anisotropy assay indicates that the presence of 5′-dsDNA does not enhance the affinity for DnaX-complex. DNA substrates with a tailed DNA (only 3′-end) (left), with a 10-nt gap (middle), and with a 30-nt gapped (right) had a similar affinity of 118 nM, 97 nM, and 94 nM, respectively, for the DnaX-complex. The fluorescence intensity signal was normalized (I /I0) for each fluorescent DNA template in the absence of the ligand. Assays were performed in triplicate. The apparent K_d ($^{App}K_d$) values are presented as mean values (black triangles) ± the standard deviations (error bars). (**C**) Rate of clamp loading onto a DNA with only 3′-recessed end is similar to that of loading onto a 45-nt gapped DNA with both 3′- and 5′- recessed ends.

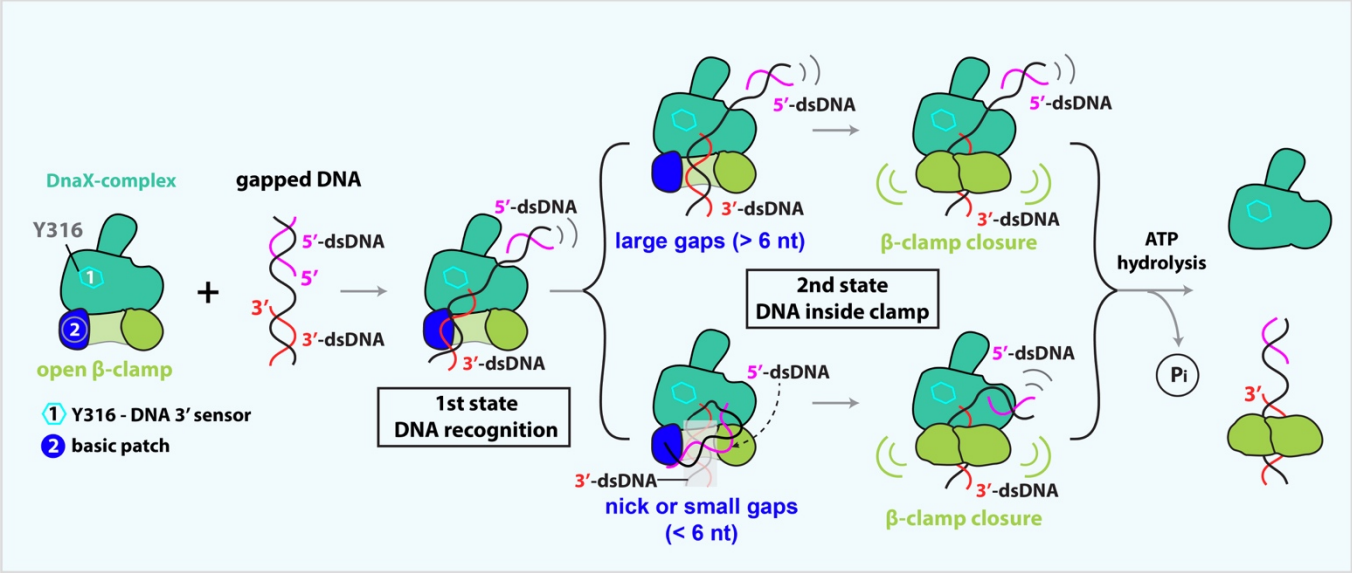

Figure 6. The DnaX-complex is proposed to load β-clamp in a DNA structure-dependent manner. The bacterial clamp loader recognizes but does not unwind the DNA recessed 3′-end via the δ Y316 residue, and the β-clamp has a basic patch on the outer surface that binds dsDNA. When a gapped DNA encounters a DnaX-complex bound to an open gate β-clamp, the 3′-dsDNA binds to the β-clamp basic patch in a tilted manner (1st state). If the gap is long enough to thread the loader (> 6 nt), the 5′-dsDNA hangs outside the loader while the 3′-dsDNA diffuses to the higher affinity β-clamp interior chamber (2nd state). Alternatively, at a nick or small-gapped DNA (< 6 nt), the 5′-dsDNA bends down towards the 3′-dsDNA, adopts a U-shape conformation, and pushes the 3′-dsDNA towards the β-clamp chamber. Once inside the clamp chamber, the 3′-dsDNA attracts the positively charged interior clamp surface to close the clamp. Finally, ATP hydrolysis dissociates DnaX-complex, leaving the β-clamp encircling the 3′-dsDNA.

772

Table 1. Cryo-EM data collection, refinement, and atomic model validation

Structures	DnaX-complex–β-clamp–1-nt gapped DNA					DnaX-complex[a]	ψ-χ focus refined[a]
	State 1 conf. 1	State 1 conf. 2	State 1 conf. 3	State 2 conf. 1	State 2 conf. 2		
EMDB ID	EMD-71013	EMD-71014	EMD-71015	EMD-71016	EMD-71017	EMD-71018	EMD-71020
PDB ID	9OYB	9OYC	9OYD	9OYE	9OYF	9OYG	
Data collection							
Magnification	105,000						
Voltage (kV)	300						
Dose ($e^-/Å^2$)	49.6					59	
Under-focus (μm)	1.2 - 1.6						
Pixel size (Å)	0.828						
Symmetry	C1						
Initial particle #	4.1 million					3.1 M	7.8 M
Final particle #	105,100	228,387	232,057	283,092	203,554	478,123	242,505
Map resolution (Å)	3.14	2.71	2.73	2.72	3.12	2.95	5.50
FSC threshold						0.143	
Map resolution range (Å)	2.7 – 11.0	2.4 – 11.0	2.3 – 12.0	2.4 – 10.3	2.7 – 10.1	2.5 – 9.5	4.5 – 13.0
Refinement							
Initial model used (PDB code)	1JR3, 3BEP					1JR3	3SXU
Map sharpening B factor ($Å^2$)	-105.2	-86.9	-87.1	-99.5	-107.2	-116.7	-211.4
Map to model CC_{mask}	0.89	0.89	0.88	0.88	0.88	0.79	
Model composition							
Non-hydrogen atoms	21,074	20,894	20,661	21,517	21,127	14,125	
Protein and DNA residues	2,532; 59	2,530; 51	2,529; 40	2,531; 81	2,531; 62	1794; 0	
Ligands	10	10	10	10	10	10	
R.m.s. deviations							
Bond lengths (Å)	0.004	0.004	0.003	0.006	0.005	0.003	
Bond angels (°)	0.756	0.631	0.594	0.684	0.669	0.623	
Validation							
MolProbity score	1.34	1.67	1.26	1.38	1.49	1.58	
Clashscore	5.53	4.56	4.99	6.08	5.47	8.42	
Poor rotamers (%)	0	0	0	0	0	0	
Ramachandran plot							
Favored (%)	97.81	98.33	98.29	97.77	96.86	97.35	
Allowed (%)	2.19	1.67	1.71	2.23	3.14	2.65	
Disallowed (%)	0	0	0	0	0	0	

773 [a]: The last two columns are from dataset with 10-nt gapped DNA (continued in **Table S2**).

REFERENCES

1. Stukenberg, P.T., Studwell-Vaughan, P.S., and O'Donnell, M. (1991). Mechanism of the sliding beta-clamp of DNA polymerase III holoenzyme. J Biol Chem *266*, 11328-11334.
2. Kong, X.P., Onrust, R., O'Donnell, M., and Kuriyan, J. (1992). Three-dimensional structure of the beta subunit of E. coli DNA polymerase III holoenzyme: a sliding DNA clamp. Cell *69*, 425-437. 10.1016/0092-8674(92)90445-i.
3. Kelch, B.A., Makino, D.L., O'Donnell, M., and Kuriyan, J. (2012). Clamp loader ATPases and the evolution of DNA replication machinery. BMC Biol *10*, 34. 10.1186/1741-7007-10-34.
4. O'Donnell, M., Langston, L., and Stillman, B. (2013). Principles and concepts of DNA replication in bacteria, archaea, and eukarya. Cold Spring Harb Perspect Biol *5*. 10.1101/cshperspect.a010108.
5. Krishna, T.S., Kong, X.P., Gary, S., Burgers, P.M., and Kuriyan, J. (1994). Crystal structure of the eukaryotic DNA polymerase processivity factor PCNA. Cell *79*, 1233-1243. 10.1016/0092-8674(94)90014-0.
6. Gulbis, J.M., Kelman, Z., Hurwitz, J., O'Donnell, M., and Kuriyan, J. (1996). Structure of the C-terminal region of p21(WAF1/CIP1) complexed with human PCNA. Cell *87*, 297-306. 10.1016/s0092-8674(00)81347-1.
7. Jeruzalmi, D., O'Donnell, M., and Kuriyan, J. (2001). Crystal structure of the processivity clamp loader gamma (gamma) complex of E. coli DNA polymerase III. Cell *106*, 429-441. 10.1016/s0092-8674(01)00463-9.
8. Johnson, A., and O'Donnell, M. (2005). Cellular DNA replicases: components and dynamics at the replication fork. Annu Rev Biochem *74*, 283-315. 10.1146/annurev.biochem.73.011303.073859.
9. Ellison, V., and Stillman, B. (1998). Reconstitution of recombinant human replication factor C (RFC) and identification of an RFC subcomplex possessing DNA-dependent ATPase activity. J Biol Chem *273*, 5979-5987. 10.1074/jbc.273.10.5979.
10. Bowman, G.D., O'Donnell, M., and Kuriyan, J. (2004). Structural analysis of a eukaryotic sliding DNA clamp-clamp loader complex. Nature *429*, 724-730. 10.1038/nature02585.
11. Kelch, B., Makino, D., Simonetta, K., O'Donnell, M., and Kuriyan, J. (2012). Molecular Mechanisms of DNA Polymerase Clamp Loaders. Macromolecular Crystallography, 103-114.
12. Gaubitz, C., Liu, X., Pajak, J., Stone, N.P., Hayes, J.A., Demo, G., and Kelch, B.A. (2022). Cryo-EM structures reveal high-resolution mechanism of a DNA polymerase sliding clamp loader. Elife *11*. 10.7554/eLife.74175.
13. Zheng, F., Georgescu, R., Yao, N.Y., Li, H., and O'Donnell, M.E. (2022). Cryo-EM structures reveal that RFC recognizes both the 3'- and 5'-DNA ends to load PCNA onto gaps for DNA repair. Elife *11*. 10.7554/eLife.77469.
14. Liu, X., Gaubitz, C., Pajak, J., and Kelch, B.A. (2022). A second DNA binding site on RFC facilitates clamp loading at gapped or nicked DNA. Elife *11*. 10.7554/eLife.77483.
15. Schrecker, M., Castaneda, J.C., Devbhandari, S., Kumar, C., Remus, D., and Hite, R.K. (2022). Multistep loading of a DNA sliding clamp onto DNA by replication factor C. Elife *11*. 10.7554/eLife.78253.
16. Xu, Z.Q., Jergic, S., Lo, A.T.Y., Pradhan, A.C., Brown, S.H.J., Bouwer, J.C., Ghodke, H., Lewis, P.J., Tolun, G., Oakley, A.J., and Dixon, N.E. (2024). Structural characterisation of the complete cycle of sliding clamp loading in Escherichia coli. Nat Commun *15*, 8372. 10.1038/s41467-024-52623-9.
17. Landeck, J.T., Pajak, J., Norman, E.K., Sedivy, E.L., and Kelch, B.A. (2024). Differences between bacteria and eukaryotes in clamp loader mechanism, a conserved process underlying DNA replication. J Biol Chem *300*, 107166. 10.1016/j.jbc.2024.107166.
18. Turner, J., Hingorani, M.M., Kelman, Z., and O'Donnell, M. (1999). The internal workings of a DNA polymerase clamp-loading machine. EMBO J *18*, 771-783. 10.1093/emboj/18.3.771.
19. Johnson, A., and O'Donnell, M. (2003). Ordered ATP hydrolysis in the gamma complex clamp loader AAA+ machine. J Biol Chem *278*, 14406-14413. 10.1074/jbc.M212708200.
20. Johnson, A., Yao, N.Y., Bowman, G.D., Kuriyan, J., and O'Donnell, M. (2006). The replication factor C clamp loader requires arginine finger sensors to drive DNA binding and proliferating cell nuclear antigen loading. J Biol Chem *281*, 35531-35543. 10.1074/jbc.M606090200.

21. Li, H., O'Donnell, M., and Kelch, B. (2022). Unexpected new insights into DNA clamp loaders: Eukaryotic clamp loaders contain a second DNA site for recessed 5' ends that facilitates repair and signals DNA damage: Eukaryotic clamp loaders contain a second DNA site for recessed 5' ends that facilitates repair and signals DNA damage. Bioessays *44*, e2200154. 10.1002/bies.202200154.
22. Liu, J., Zhou, Y., and Hingorani, M.M. (2017). Linchpin DNA-binding residues serve as go/no-go controls in the replication factor C-catalyzed clamp-loading mechanism. J Biol Chem *292*, 15892-15906. 10.1074/jbc.M117.798702.
23. Marzahn, M.R., Hayner, J.N., Meyer, J.A., and Bloom, L.B. (2015). Kinetic analysis of PCNA clamp binding and release in the clamp loading reaction catalyzed by Saccharomyces cerevisiae replication factor C. Biochim Biophys Acta *1854*, 31-38. 10.1016/j.bbapap.2014.09.019.
24. Sakato, M., Zhou, Y., and Hingorani, M.M. (2012). ATP binding and hydrolysis-driven rate-determining events in the RFC-catalyzed PCNA clamp loading reaction. J Mol Biol *416*, 176-191. 10.1016/j.jmb.2011.12.018.
25. Zheng, F., Georgescu, R.E., Yao, N.Y., O'Donnell, M.E., and Li, H. (2022). DNA is loaded through the 9-1-1 DNA checkpoint clamp in the opposite direction of the PCNA clamp. Nat Struct Mol Biol *29*, 376-385. 10.1038/s41594-022-00742-6.
26. Castaneda, J.C., Schrecker, M., Remus, D., and Hite, R.K. (2022). Mechanisms of loading and release of the 9-1-1 checkpoint clamp. Nat Struct Mol Biol *29*, 369-375. 10.1038/s41594-022-00741-7.
27. Day, M., Oliver, A.W., and Pearl, L.H. (2022). Structure of the human RAD17-RFC clamp loader and 9-1-1 checkpoint clamp bound to a dsDNA-ssDNA junction. Nucleic Acids Res *50*, 8279-8289. 10.1093/nar/gkac588.
28. Yuzhakov, A., Turner, J., and O'Donnell, M. (1996). Replisome assembly reveals the basis for asymmetric function in leading and lagging strand replication. Cell *86*, 877-886. 10.1016/s0092-8674(00)80163-4.
29. Zheng, F., Georgescu, R.E., Yao, N.Y., O'Donnell, M.E., and Li, H. (2023). Structures of 9-1-1 DNA checkpoint clamp loading at gaps from start to finish and ramification on biology. Cell Rep *42*, 112694. 10.1016/j.celrep.2023.112694.
30. Gaubitz, C., Liu, X., Magrino, J., Stone, N.P., Landeck, J., Hedglin, M., and Kelch, B.A. (2020). Structure of the human clamp loader reveals an autoinhibited conformation of a substrate-bound AAA+ switch. Proc Natl Acad Sci U S A *117*, 23571-23580. 10.1073/pnas.2007437117.
31. Simonetta, K.R., Kazmirski, S.L., Goedken, E.R., Cantor, A.J., Kelch, B.A., McNally, R., Seyedin, S.N., Makino, D.L., O'Donnell, M., and Kuriyan, J. (2009). The mechanism of ATP-dependent primer-template recognition by a clamp loader complex. Cell *137*, 659-671. 10.1016/j.cell.2009.03.044.
32. Marceau, A.H., Bahng, S., Massoni, S.C., George, N.P., Sandler, S.J., Marians, K.J., and Keck, J.L. (2011). Structure of the SSB-DNA polymerase III interface and its role in DNA replication. EMBO J *30*, 4236-4247. 10.1038/emboj.2011.305.
33. Tondnevis, F., Gillilan, R.E., Bloom, L.B., and McKenna, R. (2015). Solution study of the Escherichia coli DNA polymerase III clamp loader reveals the location of the dynamic psichi heterodimer. Struct Dyn *2*, 054701. 10.1063/1.4927407.
34. Yao, N., Leu, F.P., Anjelkovic, J., Turner, J., and O'Donnell, M. (2000). DNA structure requirements for the Escherichia coli gamma complex clamp loader and DNA polymerase III holoenzyme. J Biol Chem *275*, 11440-11450. 10.1074/jbc.275.15.11440.
35. Ason, B., Handayani, R., Williams, C.R., Bertram, J.G., Hingorani, M.M., O'Donnell, M., Goodman, M.F., and Bloom, L.B. (2003). Mechanism of loading the Escherichia coli DNA polymerase III beta sliding clamp on DNA. Bona fide primer/templates preferentially trigger the gamma complex to hydrolyze ATP and load the clamp. J Biol Chem *278*, 10033-10040. 10.1074/jbc.M211741200.
36. Snyder, A.K., Williams, C.R., Johnson, A., O'Donnell, M., and Bloom, L.B. (2004). Mechanism of loading the Escherichia coli DNA polymerase III sliding clamp: II. Uncoupling the beta and DNA binding activities of the gamma complex. J Biol Chem *279*, 4386-4393. 10.1074/jbc.M310430200.
37. Rajagopalan, M., Lu, C., Woodgate, R., O'Donnell, M., Goodman, M.F., and Echols, H. (1992). Activity of the purified mutagenesis proteins UmuC, UmuD', and RecA in replicative bypass of an

881 abasic DNA lesion by DNA polymerase III. Proc Natl Acad Sci U S A *89*, 10777-10781.
882 10.1073/pnas.89.22.10777.
883 38. Indiani, C., Langston, L.D., Yurieva, O., Goodman, M.F., and O'Donnell, M. (2009). Translesion
884 DNA polymerases remodel the replisome and alter the speed of the replicative helicase. Proc Natl
885 Acad Sci U S A *106*, 6031-6038. 10.1073/pnas.0901403106.
886 39. Indiani, C., McInerney, P., Georgescu, R., Goodman, M.F., and O'Donnell, M. (2005). A sliding-
887 clamp toolbelt binds high- and low-fidelity DNA polymerases simultaneously. Mol Cell *19*, 805-815.
888 10.1016/j.molcel.2005.08.011.
889 40. Indiani, C., Patel, M., Goodman, M.F., and O'Donnell, M.E. (2013). RecA acts as a switch to
890 regulate polymerase occupancy in a moving replication fork. Proc Natl Acad Sci U S A *110*, 5410-
891 5415. 10.1073/pnas.1303301110.
892 41. Bonner, C.A., Stukenberg, P.T., Rajagopalan, M., Eritja, R., O'Donnell, M., McEntee, K., Echols,
893 H., and Goodman, M.F. (1992). Processive DNA synthesis by DNA polymerase II mediated by DNA
894 polymerase III accessory proteins. J Biol Chem *267*, 11431-11438.
895 42. Wagner, J., Fujii, S., Gruz, P., Nohmi, T., and Fuchs, R.P. (2000). The beta clamp targets DNA
896 polymerase IV to DNA and strongly increases its processivity. EMBO Rep *1*, 484-488.
897 10.1093/embo-reports/kvd109.
898 43. Bloom, L.B. (2009). Loading clamps for DNA replication and repair. DNA Repair (Amst) *8*, 570-578.
899 10.1016/j.dnarep.2008.12.014.
900 44. Lopez de Saro, F.J., and O'Donnell, M. (2001). Interaction of the beta sliding clamp with MutS,
901 ligase, and DNA polymerase I. Proc Natl Acad Sci U S A *98*, 8376-8380. 10.1073/pnas.121009498.
902 45. Becherel, O.J., Fuchs, R.P., and Wagner, J. (2002). Pivotal role of the beta-clamp in translesion
903 DNA synthesis and mutagenesis in E. coli cells. DNA Repair (Amst) *1*, 703-708. 10.1016/s1568-
904 7864(02)00106-4.
905 46. Yang, W. (2003). Damage repair DNA polymerases Y. Curr Opin Struct Biol *13*, 23-30.
906 10.1016/s0959-440x(02)00003-9.
907 47. Maul, R.W., Ponticelli, S.K., Duzen, J.M., and Sutton, M.D. (2007). Differential binding of
908 Escherichia coli DNA polymerases to the beta-sliding clamp. Mol Microbiol *65*, 811-827.
909 10.1111/j.1365-2958.2007.05828.x.
910 48. Maslowska, K.H., Makiela-Dzbenska, K., and Fijalkowska, I.J. (2019). The SOS system: A complex
911 and tightly regulated response to DNA damage. Environ Mol Mutagen *60*, 368-384.
912 10.1002/em.22267.
913 49. Martinez, B., Bharati, B.K., Epshtein, V., and Nudler, E. (2022). Pervasive Transcription-coupled
914 DNA repair in E. coli. Nat Commun *13*, 1702. 10.1038/s41467-022-28871-y.
915 50. Kath, J.E., Chang, S., Scotland, M.K., Wilbertz, J.H., Jergic, S., Dixon, N.E., Sutton, M.D., and
916 Loparo, J.J. (2016). Exchange between Escherichia coli polymerases II and III on a processivity
917 clamp. Nucleic Acids Res *44*, 1681-1690. 10.1093/nar/gkv1375.
918 51. Furukohri, A., Goodman, M.F., and Maki, H. (2008). A dynamic polymerase exchange with
919 Escherichia coli DNA polymerase IV replacing DNA polymerase III on the sliding clamp. J Biol
920 Chem *283*, 11260-11269. 10.1074/jbc.M709689200.
921 52. Kath, J.E., Jergic, S., Heltzel, J.M., Jacob, D.T., Dixon, N.E., Sutton, M.D., Walker, G.C., and
922 Loparo, J.J. (2014). Polymerase exchange on single DNA molecules reveals processivity clamp
923 control of translesion synthesis. Proc Natl Acad Sci U S A *111*, 7647-7652.
924 10.1073/pnas.1321076111.
925 53. Li, N., Lam, W.H., Zhai, Y., Cheng, J., Cheng, E., Zhao, Y., Gao, N., and Tye, B.K. (2018). Structure
926 of the origin recognition complex bound to DNA replication origin. Nature *559*, 217-222.
927 10.1038/s41586-018-0293-x.
928 54. Correction for Yuan et al., Structural mechanism of helicase loading onto replication origin DNA by
929 ORC-Cdc6. (2021). Proc Natl Acad Sci U S A *118*. 10.1073/pnas.2025413118.
930 55. Neylon, C., Kralicek, A.V., Hill, T.M., and Dixon, N.E. (2005). Replication termination in Escherichia
931 coli: structure and antihelicase activity of the Tus-Ter complex. Microbiol Mol Biol Rev *69*, 501-526.
932 10.1128/MMBR.69.3.501-526.2005.

56. Simonsen, S., Sogaard, C.K., Olsen, J.G., Otterlei, M., and Kragelund, B.B. (2024). The bacterial DNA sliding clamp, beta-clamp: structure, interactions, dynamics and drug discovery. Cell Mol Life Sci *81*, 245. 10.1007/s00018-024-05252-w.
57. Moolman, M.C., Krishnan, S.T., Kerssemakers, J.W., van den Berg, A., Tulinski, P., Depken, M., Reyes-Lamothe, R., Sherratt, D.J., and Dekker, N.H. (2014). Slow unloading leads to DNA-bound beta2-sliding clamp accumulation in live Escherichia coli cells. Nat Commun *5*, 5820. 10.1038/ncomms6820.
58. Lazowski, K., Woodgate, R., and Fijalkowska, I.J. (2024). Escherichia coli DNA replication: the old model organism still holds many surprises. FEMS Microbiol Rev *48*. 10.1093/femsre/fuae018.
59. Fernandez-Leiro, R., Conrad, J., Scheres, S.H.W., and Lamers, M.H. (2015). cryo-EM structures of the E. coli replicative DNA polymerase reveal its dynamic interactions with the DNA sliding clamp, exonuclease and τ. eLife *4*, e11134. 10.7554/eLife.11134.
60. Reyes-Lamothe, R., Sherratt, D.J., and Leake, M.C. (2010). Stoichiometry and architecture of active DNA replication machinery in Escherichia coli. Science *328*, 498-501. 10.1126/science.1185757.
61. McInerney, P., Johnson, A., Katz, F., and O'Donnell, M. (2007). Characterization of a triple DNA polymerase replisome. Mol Cell *27*, 527-538. 10.1016/j.molcel.2007.06.019.
62. Kelman, Z., Yao, N., and O'Donnell, M. (1995). Escherichia coli expression vectors containing a protein kinase recognition motif, His6-tag and hemagglutinin epitope. Gene *166*, 177-178. 10.1016/0378-1119(95)00556-7.
63. Onrust, R., Finkelstein, J., Naktinis, V., Turner, J., Fang, L., and O'Donnell, M. (1995). Assembly of a chromosomal replication machine: two DNA polymerases, a clamp loader, and sliding clamps in one holoenzyme particle. I. Organization of the clamp loader. J Biol Chem *270*, 13348-13357. 10.1074/jbc.270.22.13348.
64. Studwell, P.S., and O'Donnell, M. (1990). Processive replication is contingent on the exonuclease subunit of DNA polymerase III holoenzyme. J Biol Chem *265*, 1171-1178.
65. Mastronarde, D.N. (2003). SerialEM: A Program for Automated Tilt Series Acquisition on Tecnai Microscopes Using Prediction of Specimen Position. Microscopy and Microanalysis *9*, 1182 - 1183.
66. Punjani, A., Rubinstein, J.L., Fleet, D.J., and Brubaker, M.A. (2017). cryoSPARC: algorithms for rapid unsupervised cryo-EM structure determination. Nat Methods *14*, 290-296. 10.1038/nmeth.4169.
67. Scheres, S.H. (2012). RELION: implementation of a Bayesian approach to cryo-EM structure determination. J Struct Biol *180*, 519-530. 10.1016/j.jsb.2012.09.006.
68. Zheng, S.Q., Palovcak, E., Armache, J.P., Verba, K.A., Cheng, Y., and Agard, D.A. (2017). MotionCor2: anisotropic correction of beam-induced motion for improved cryo-electron microscopy. Nat Methods *14*, 331-332. 10.1038/nmeth.4193.
69. Rohou, A., and Grigorieff, N. (2015). CTFFIND4: Fast and accurate defocus estimation from electron micrographs. J Struct Biol *192*, 216-221. 10.1016/j.jsb.2015.08.008.
70. Bepler, T., Morin, A., Rapp, M., Brasch, J., Shapiro, L., Noble, A.J., and Berger, B. (2019). Positive-unlabeled convolutional neural networks for particle picking in cryo-electron micrographs. Nat Methods *16*, 1153-1160. 10.1038/s41592-019-0575-8.
71. Asarnow, D., Palovcak, E., and Cheng, Y. (2019). UCSF pyem v0. 5. Zenodo https://doi.org/10.5281/zenodo *3576630*.
72. Pettersen, E.F., Goddard, T.D., Huang, C.C., Couch, G.S., Greenblatt, D.M., Meng, E.C., and Ferrin, T.E. (2004). UCSF Chimera--a visualization system for exploratory research and analysis. J Comput Chem *25*, 1605-1612. 10.1002/jcc.20084.
73. Goddard, T.D., Huang, C.C., Meng, E.C., Pettersen, E.F., Couch, G.S., Morris, J.H., and Ferrin, T.E. (2018). UCSF ChimeraX: Meeting modern challenges in visualization and analysis. Protein Sci *27*, 14-25. 10.1002/pro.3235.
74. Emsley, P., Lohkamp, B., Scott, W.G., and Cowtan, K. (2010). Features and development of Coot. Acta Crystallogr D Biol Crystallogr *66*, 486-501. 10.1107/S0907444910007493.
75. Adams, P.D., Afonine, P.V., Bunkoczi, G., Chen, V.B., Davis, I.W., Echols, N., Headd, J.J., Hung, L.W., Kapral, G.J., Grosse-Kunstleve, R.W., et al. (2010). PHENIX: a comprehensive Python-based

system for macromolecular structure solution. Acta Crystallogr D Biol Crystallogr *66*, 213-221. 10.1107/S0907444909052925.

76. Kelman, Z., Naktinis, V., and O'Donnell, M. (1995). Radiolabeling of proteins for biochemical studies. Methods Enzymol *262*, 430-442. 10.1016/0076-6879(95)62034-6.

77. Yao, N., Turner, J., Kelman, Z., Stukenberg, P.T., Dean, F., Shechter, D., Pan, Z.Q., Hurwitz, J., and O'Donnell, M. (1996). Clamp loading, unloading and intrinsic stability of the PCNA, beta and gp45 sliding clamps of human, E. coli and T4 replicases. Genes Cells *1*, 101-113. 10.1046/j.1365-2443.1996.07007.x.

78. Zheng, F., Yao, N.Y., Georgescu, R.E., Li, H., and O'Donnell, M.E. (2024). Structure of the PCNA unloader Elg1-RFC. Sci Adv *10*, eadl1739. 10.1126/sciadv.adl1739.

79. Zheng, F., Georgescu, R.E., Li, H., and O'Donnell, M.E. (2020). Structure of eukaryotic DNA polymerase delta bound to the PCNA clamp while encircling DNA. Proc Natl Acad Sci U S A *117*, 30344-30353. 10.1073/pnas.2017637117.

80. Sanchez-Garcia, R., Gomez-Blanco, J., Cuervo, A., Carazo, J.M., Sorzano, C.O.S., and Vargas, J. (2021). DeepEMhancer: a deep learning solution for cryo-EM volume post-processing. Commun Biol *4*, 874. 10.1038/s42003-021-02399-1.

81. He, J., Li, T., and Huang, S.Y. (2023). Improvement of cryo-EM maps by simultaneous local and non-local deep learning. Nat Commun *14*, 3217. 10.1038/s41467-023-39031-1.

82. Asarnow, D., Palovcak, E., and Cheng, Y. (2019). UCSF pyem v0. 5. Zenodo *3576630*. https://doi.org/10.5281/zenodo.3576630.

83. Schwab, J., Kimanius, D., Burt, A., Dendooven, T., and Scheres, S.H.W. (2024). DynaMight: estimating molecular motions with improved reconstruction from cryo-EM images. Nat Methods *21*, 1855-1862. 10.1038/s41592-024-02377-5.

84. Georgescu, R.E., Kim, S.-S., Yurieva, O., Kuriyan, J., Kong, X.-P., and O'Donnell, M. (2008). Structure of a Sliding Clamp on DNA. Cell *132*, 43-54. https://doi.org/10.1016/j.cell.2007.11.045.

85. Jamali, K., Kall, L., Zhang, R., Brown, A., Kimanius, D., and Scheres, S.H.W. (2024). Automated model building and protein identification in cryo-EM maps. Nature *628*, 450-457. 10.1038/s41586-024-07215-4.

86. Chen, V.B., Arendall, W.B., 3rd, Headd, J.J., Keedy, D.A., Immormino, R.M., Kapral, G.J., Murray, L.W., Richardson, J.S., and Richardson, D.C. (2010). MolProbity: all-atom structure validation for macromolecular crystallography. Acta Crystallogr D Biol Crystallogr *66*, 12-21. 10.1107/S0907444909042073.

87. Pettersen, E.F., Goddard, T.D., Huang, C.C., Meng, E.C., Couch, G.S., Croll, T.I., Morris, J.H., and Ferrin, T.E. (2021). UCSF ChimeraX: Structure visualization for researchers, educators, and developers. Protein Sci *30*, 70-82. 10.1002/pro.3943.

88. Oakley, A.J., Prosselkov, P., Wijffels, G., Beck, J.L., Wilce, M.C., and Dixon, N.E. (2003). Flexibility revealed by the 1.85 A crystal structure of the beta sliding-clamp subunit of Escherichia coli DNA polymerase III. Acta Crystallogr D Biol Crystallogr *59*, 1192-1199. 10.1107/s0907444903009958.

89. Kimanius, D., Jamali, K., Wilkinson, M.E., Lövestam, S., Velazhahan, V., Nakane, T., and Scheres, S.H.W. (2023). Data-driven regularisation lowers the size barrier of cryo-EM structure determination. bioRxiv, 2023.2010.2023.563586. 10.1101/2023.10.23.563586.

90. Baldwin, P.R., and Lyumkis, D. (2020). Non-uniformity of projection distributions attenuates resolution in Cryo-EM. Prog Biophys Mol Biol *150*, 160-183. 10.1016/j.pbiomolbio.2019.09.002.

91. Stewart, J., Hingorani, M.M., Kelman, Z., and O'Donnell, M. (2001). Mechanism of beta clamp opening by the delta subunit of Escherichia coli DNA polymerase III holoenzyme. J Biol Chem *276*, 19182-19189. 10.1074/jbc.M100592200.

1034 **Supplementary tables and figures**

1035
1036
1037 **Table S1. Oligonucleotides used in biochemical and cryo-EM experiments**
1038

Oligos	Sequences
Primer 1-Cy3 (for 1-nt and 10-nt gapped DNA in cryo-EM, also for binding affinity assay)	5′- GGCTCGCTACGGCTATACGG/Cy3/-3′
Primer 2 (for 1-nt and 10-nt gapped DNA in cryo-EM, also for binding affinity assay)	5′- GATTCGTATCGCCTATACCG -3
Tmpl_41-nt (for 1-nt gapped DNA in cryo-EM)	5′- CGGTATAGGCGATACGAATCTCCGTA TAGCCGTAGCG AGCC -3′
Tmpl_50-nt (for 10-nt gapped DNA in cryo-EM, also for binding affinity assay)	5′- CGGTATAGGCGATACGAATC$(T)_{10}$CCGTATAGCCGTAG CGAGCC -3′
Tmpl_70-nt (for binding affinity assay)	5′- CGGTATAGGCGATACGAATC$(T)_{30}$CCGTATAGCCGTAG CGAGCC -3′
M13 primer (for loading assay)	5′- BioTEG/GGGAAGGGCGATCGGTGCGGGCCTCTTCGCT ATTACGCCAGCTG GCGAAAGGGGGATGTGCTGCAAGGC GATTAAGTTGGGTAACGC -3′
Replication template	5′- BioTEG/CTGGATGAGTTGAGTGGACGGCTGCAGCAAGT CACCAATGTCTA AGAGTTCGTATTATGCCTACACTGGAGT ACCGGAGCATCGTCGTGACTGGGAAACT/BioTEG/ -3′
Replication primer 1	5′- AGTTTCCCAGTCACGACGATGCTCCGGTAC -3′
Replication primer 2	5′- GCAGCCGTCCACTCAACTCATCCAG -3′

1039
1040

1041 **Table S2. Cryo-EM data collection, refinement, and atomic model validation**
1042

Structures	DnaX-complex–β-clamp–10-nt gapped DNA						
	DNA recognition	**Fully open_DNA unsettled**	**Fully open_DNA settled**	**Partially closed**	**Fully closed 1**	**Fully closed 2**	**Fully closed 3**
EMDB ID	EMD-71021	EMD-71022	EMD-71023	EMD-71024	EMD-71025	EMD-71026	EMD-71027
PDB ID	9OYH	9OYI	9OYJ	9OYK	9OYL	9OYM	9OYN
Data collection and processing							
Magnification	105,000						
Voltage (kV)	300						
Electron dose (e^-/Å^2)	59						
Under-focus range (μm)	1.2 - 1.6						
Pixel size (Å)	0.828						
Symmetry imposed	C1						
Initial particle images (no.)	8,537,193						
Final particle images (no.)	473,295	502,506	499,551	476,182	360,948	539,340	443,597
Map resolution (Å)	2.54	2.54	2.53	2.60	2.88	2.60	2.70
FSC threshold	0.143						
Map resolution range (Å)	2.2 – 9.5	2.2 – 9.3	2.2 – 9.5	2.3 – 9.6	1.8 – 9.9	2.3 – 9.4	2.4 – 9.9
Refinement							
Initial model used (PDB code)	1JR3, 3BEP, 3SXU						
Map sharpening B factor (Å^2)	-91.6	-92.5	-92.6	-95.7	-99.1	-98.1	-99.0
Map to model CC_{mask}	0.71	0.87	0.75	0.87	0.75	0.86	0.82
Model composition							
Non-hydrogen atoms	22,702	20,796	20,835	20,861	20,835	20,861	20,843
Protein and DNA residues	2,779; 44	2,531; 46	2,531; 47	2,534; 47	2,532; 47	2,534; 47	2532; 47
Ligands	10	10	11	11	11	11	11
R.m.s. deviations							
Bond lengths (Å)	0.002	0.005	0.007	0.003	0.003	0.004	0.005
Bond angels (º)	0.480	0.634	0.687	0.530	0.489	0.587	0.579
Validation							
MolProbity score	1.40	1.21	1.52	1.24	1.45	1.21	1.37
Clashscore	7.29	4.31	6.67	4.73	6.98	4.25	5.19
Poor rotamers (%)	0	0	0	0	0	0	0

Ramachandran plot							
Favored (%)	98.15	98.17	97.13	98.13	97.69	98.57	97.54
Allowed (%)	1.85	1.83	2.87	1.87	2.31	1.43	2.46
Disallowed (%)	0	0	0	0	0	0	0

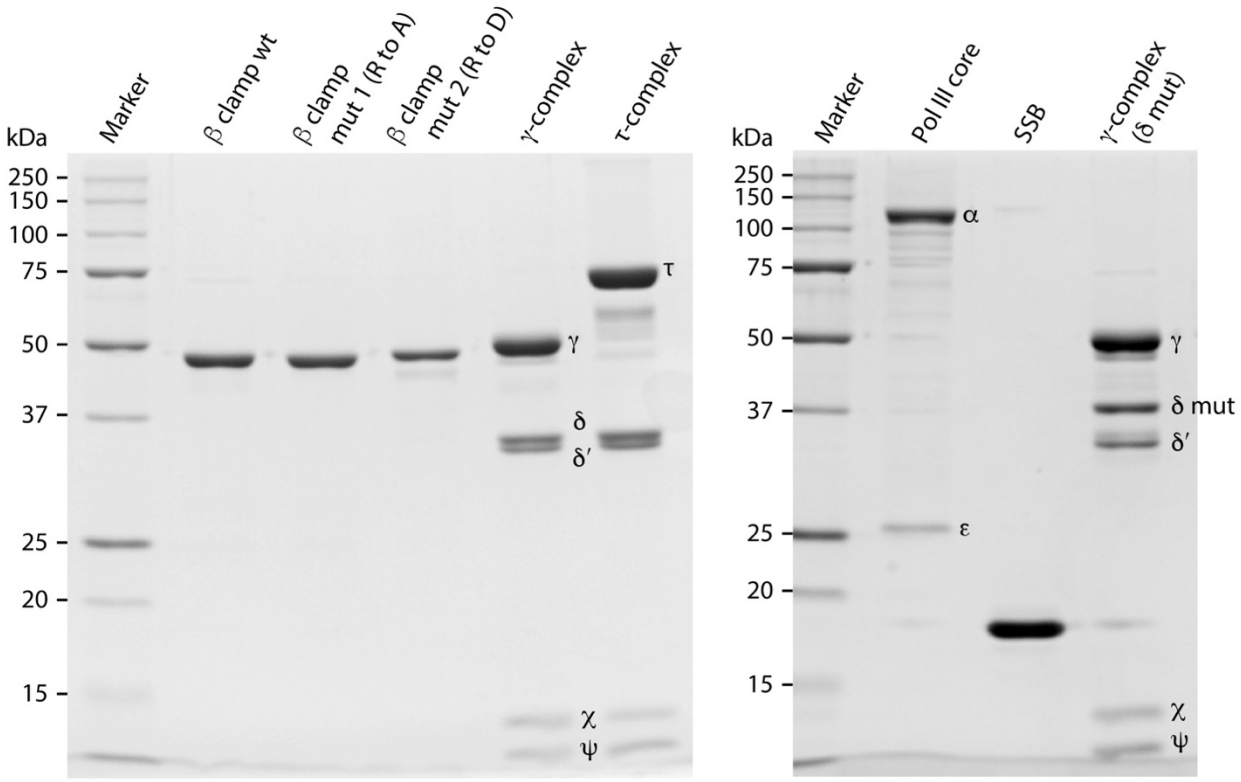

Figure S1. 12% SDS-PAGE analysis of the purified proteins used in this study, related to Figure 1. (**A**) The purified β-clamp wildtype (wt), mut 1 (with R96A, R103A, R105A mutations), mut 2 (with R96D, R103D, R105D mutations), and DnaX-complexes (γ and τ forms). (**B**) The purified polymerase III core (Pol III α and ε), SSB (single-stranded binding protein), and γ-complex harboring the Y316A mutation in δ subunit. Protein markers are shown in left of each gel (in kDa), and the position of each subunit is also labelled.

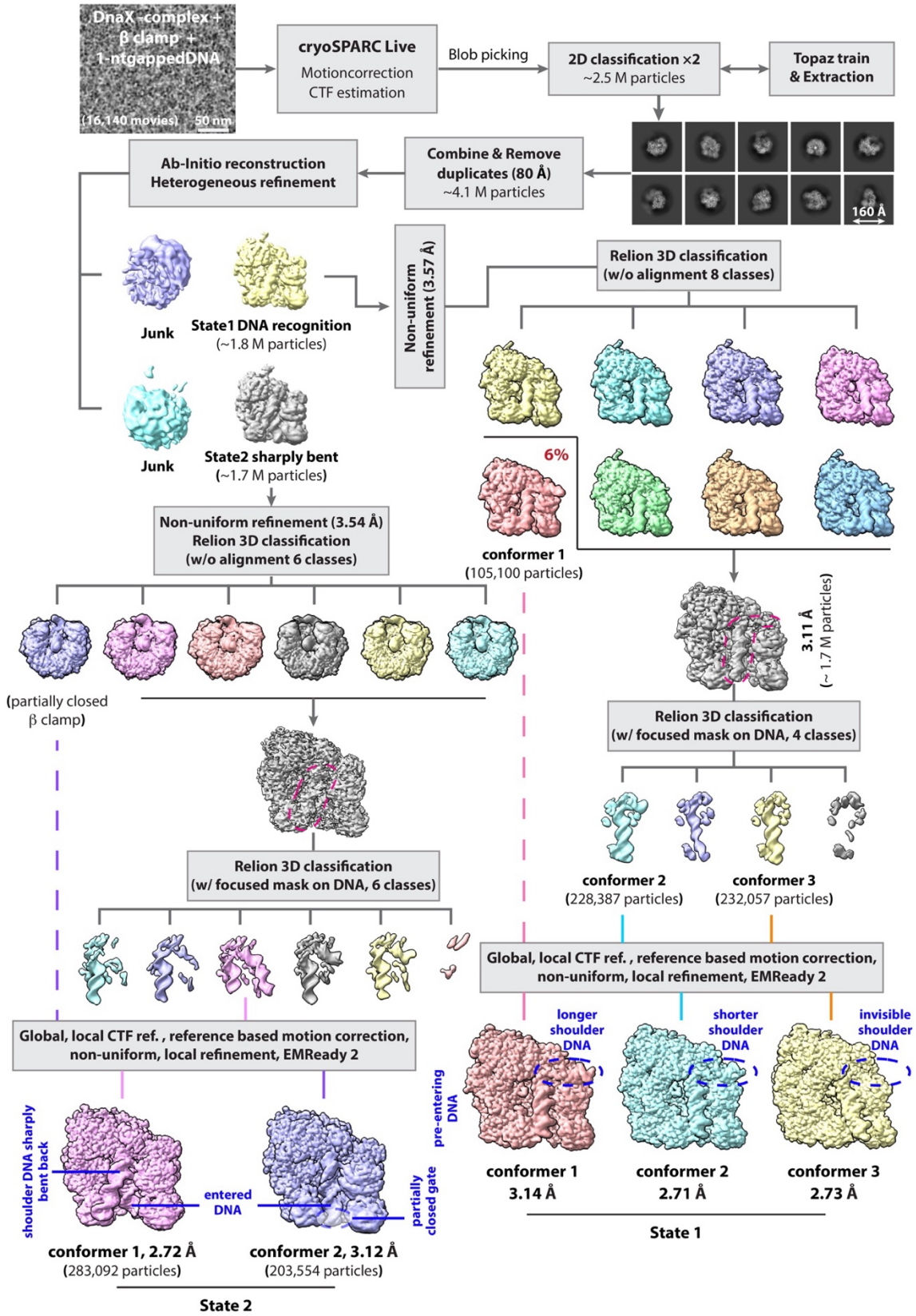

Figure S2. Cryo-EM data processing of DnaX-complex–β-clamp with 1-nt gapped DNA, related to Figures 1–2. A typical micrograph from ~16K movies collected on 300kV Titan Krios microscope is shown with scale bar. Images were processed in both cryoSPARC v4.5 and Relion v5.0[66,89]. Two major states (1st and 2nd states) were captured. The 1st state had three conformers, and the 2nd state had two conformers.

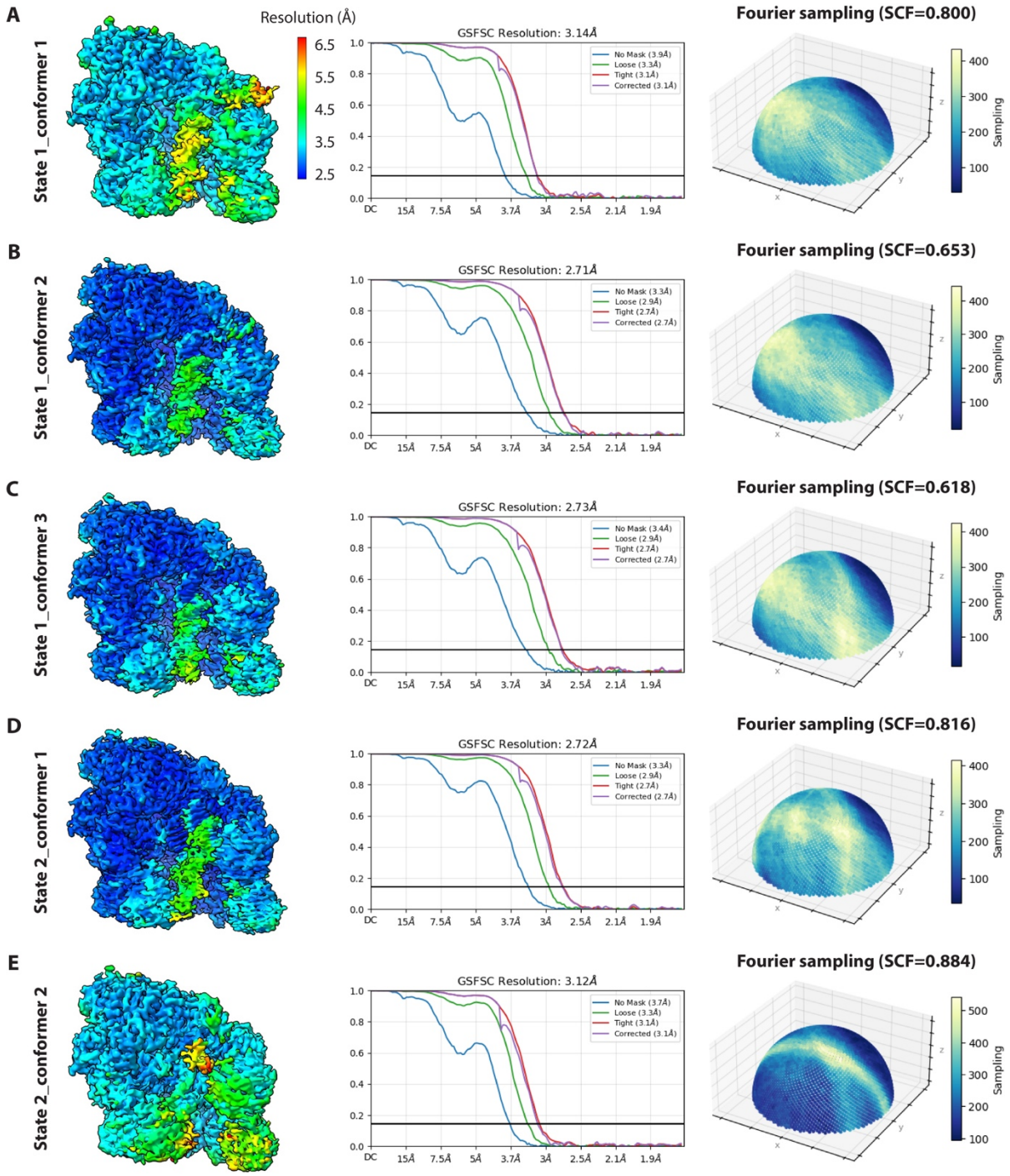

Figure S3. Characterization of the 3D cryo-EM maps derived from the DnaX-complex–β-clamp–1-nt gapped DNA assembly, related to Figures 1–2. Local resolution estimation (left), corresponding gold standard FSC curves (GSFSC, middle) and particle orientation distribution evaluated by Sampling Compensation Factor (SCF, right)[90] of maps in state 1 conformers 1–3 (**A**–**C**) and state 2 conformers 1–2 (**D**–**E**).

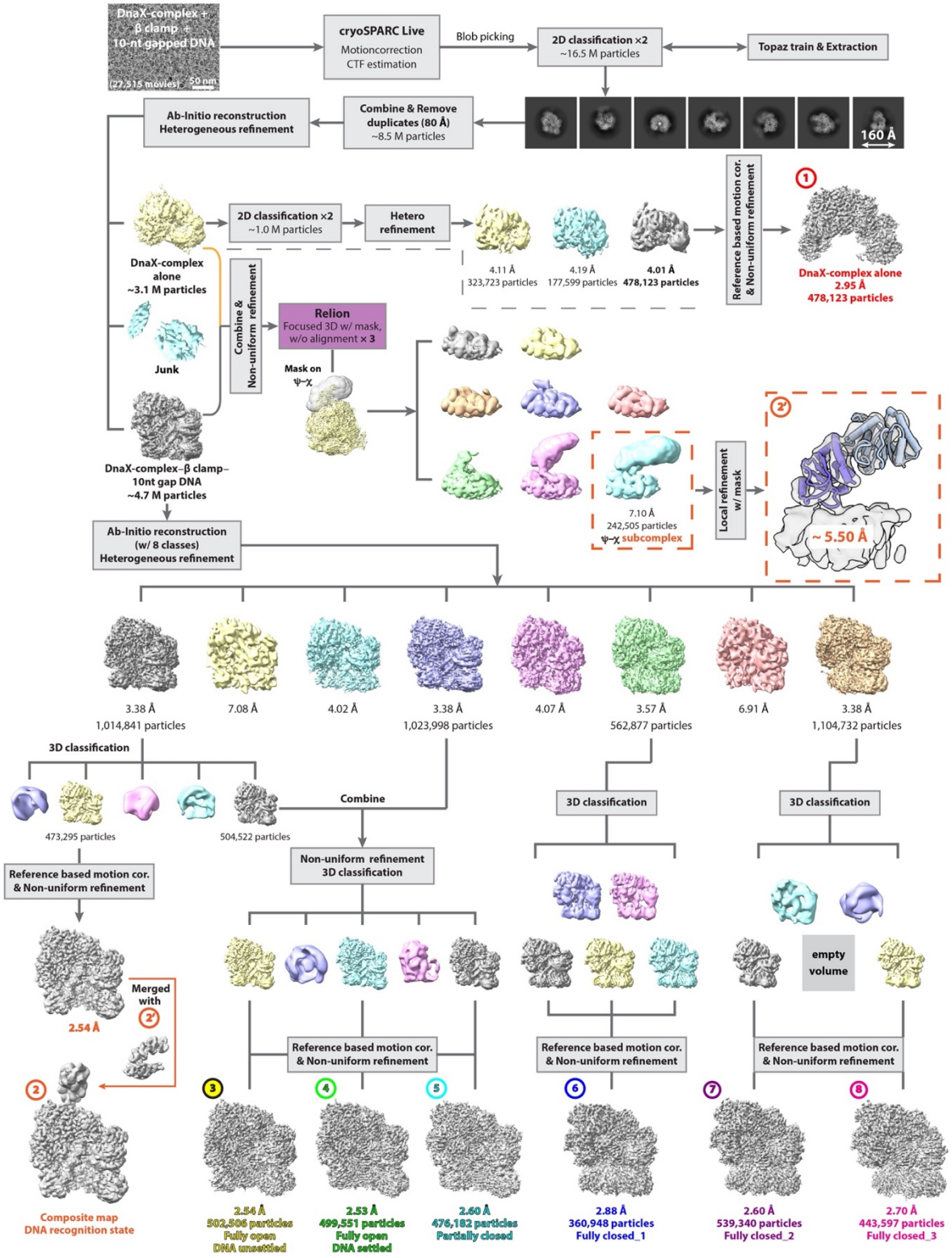

Figure S4. Cryo-EM data processing of the DnaX-complex–β-clamp with 10-nt gapped DNA, related to Figures 3–4. A typical micrograph from ~28K movies collected on 300kV Titan Krios microscope is shown with scale bar. Images were processed in both cryoSPARC v4.5 and Relion v5.0[66,89]. Eight different states (3.0 Å to 2.5 Å resolutions) are captured with ψ–χ subcomplex being merged to the state 2 map. The SSB peptide bound ψ-χ crystal structure (PDB 3SXU) was rigid-body fitted into the local refined 3D map highlighted in dashed red squares.

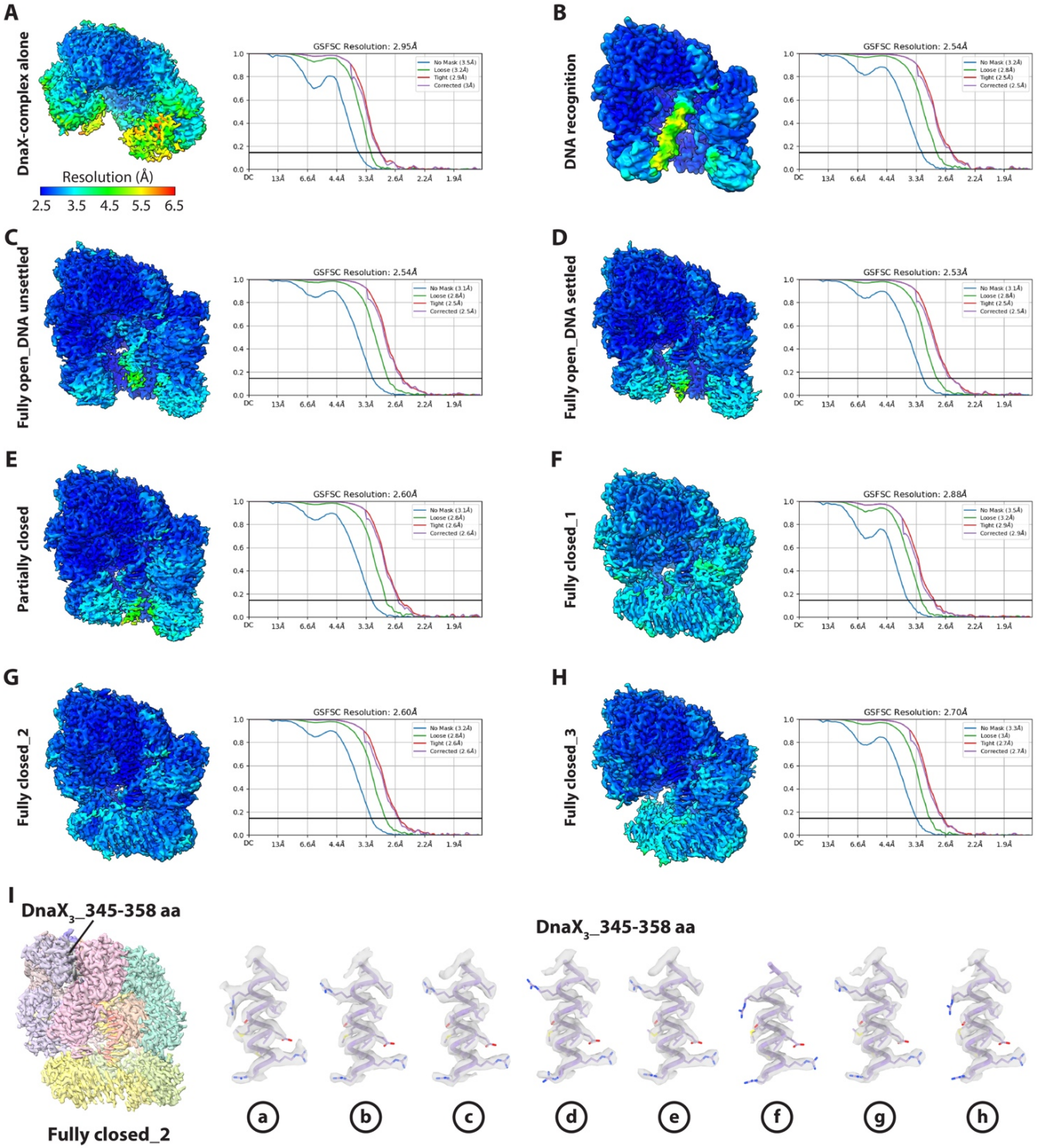

Figure S5. Characterization of the eight cryo-EM 3D maps derived from the DnaX-complex–β-clamp–10-nt gapped DNA assembly, related to Figures 3–4. (**A**–**H**) DnaX-complex alone (**A**) and seven different β-clamp loading conformers (**B**–**H**). In each panel are shown the local resolution estimation (left) and corresponding gold standard FSC curves (Right). (**I**) EM density of the same selected region from eight maps each with atomic model superimposed. The selected region is marked in the full map of the fully closed_2.

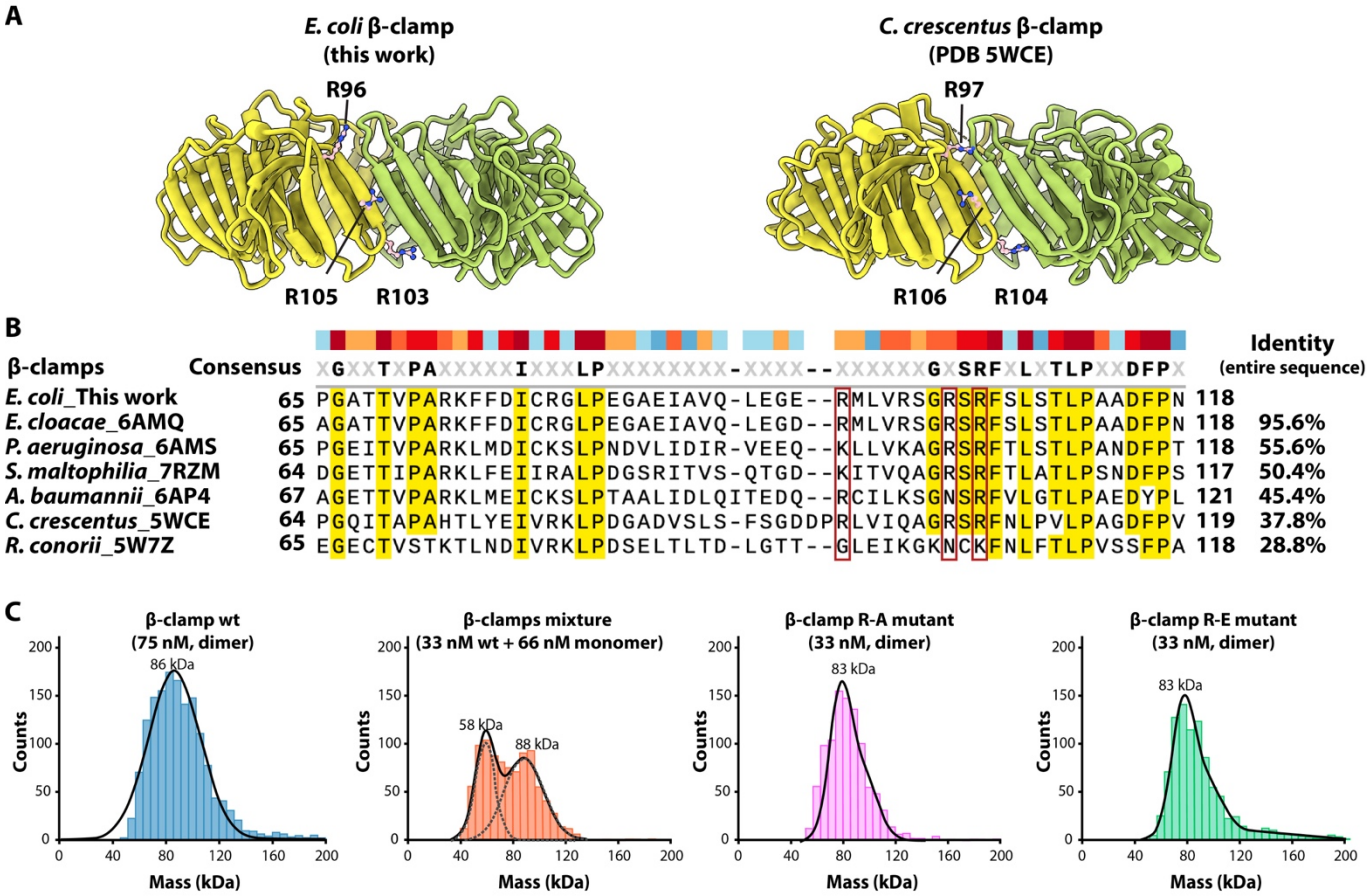

Figure S6. The basic patch on the outer surface of the β-clamp is conserved among prokaryotes. Related to Figure 3. (**A**) Structural comparison of *E. coli* β-clamp with that of *C. crescentus* as a representative. The three basic residues comprising the basic patch are shown as sticks; they are on the outer surface at the left side of the DNA entry gate between the two β subunits. (**B**) Sequence alignment in the region containing the three basic residues highlighted in the red boxes. Structures were aligned in ChimeraX[87]. The PDB code for each entry is listed following the species name. (**C**) The two β-clamp mutants used in this study remain as dimers in solution. The mass photometry (Refeyn OnePM) has a low molecular weight cut off of around 40 kDa, and therefore β monomer readings are expected to be somewhat higher than actual. As controls, we used wt β dimer and also the known β monomer in which the hydrophobic core residues are mutated to produce a monomer that does not form a dimer (I272A/L273/A)[91]. The two β-clamp mutants in which R96, R103, R105 are each changed to Ala or Glu remain dimer in solution.

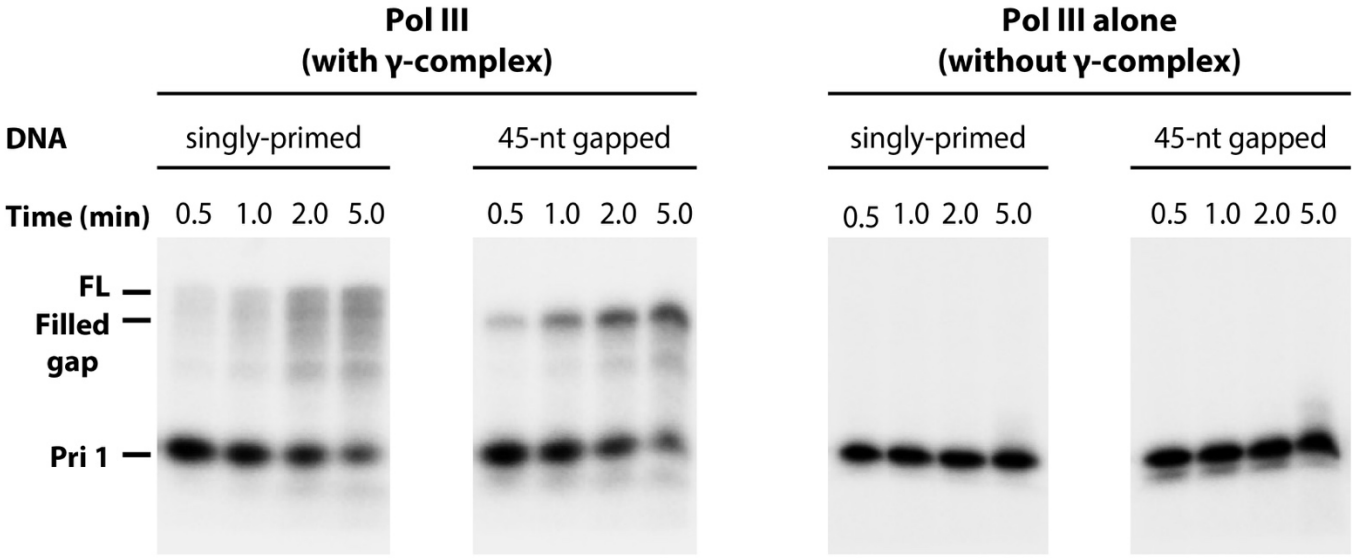

Figure S7. Urea-PAGE analysis of ^{32}P labelled primer extension at increasing times of loading using either a singly primed or gapped DNA, in the presence (left) or absence (middle) of γ-complex. Note, A sufficient amount of Pol III was added to saturate the reaction, making clamp loading the rate limiting step.

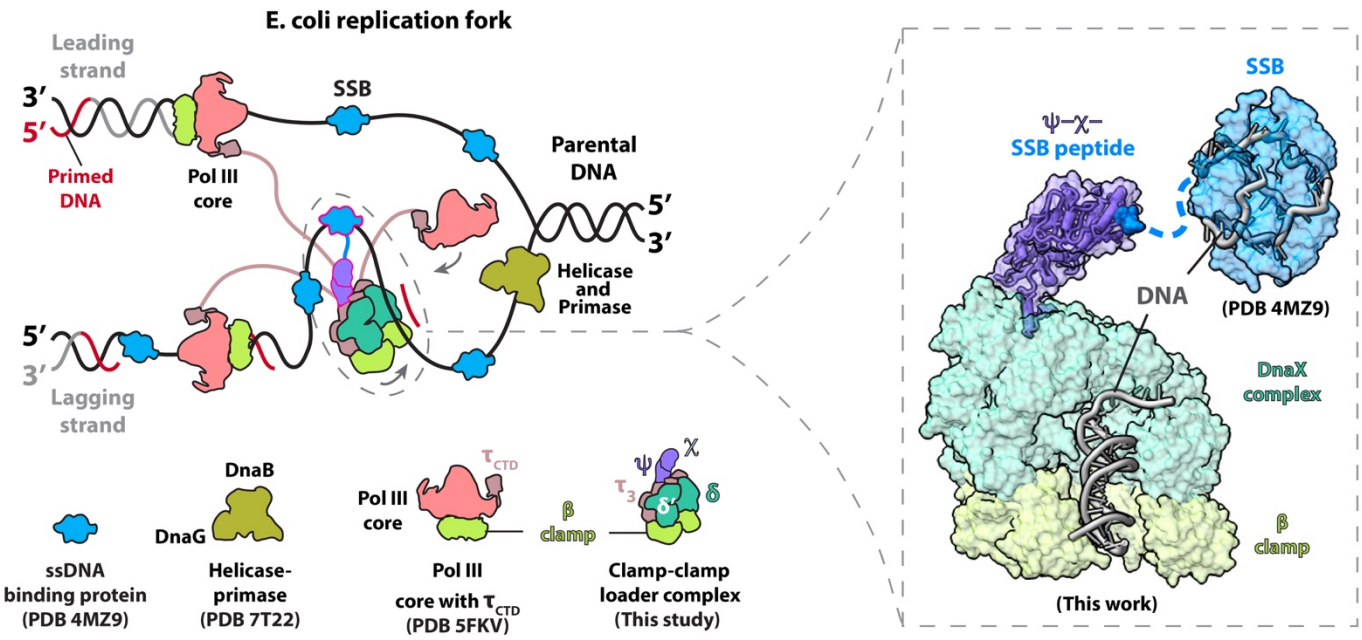

Figure S8. A sketch showing how DnaX-holo-complex may coordinate the replisome, related to Figure 6. In the left panel is shown a simplified model of the *E. coli* replication fork, including the DnaB helicase encircling the lagging strand and unwinding parental DNA, the DnaG primase bound to the helicase making RNA primers on the lagging strand template, and several SSB molecules coating the ssDNA. In addition to loading the β-clamp for the two Pol III in the leading and lagging strand DNA, the DnaX-holo-complex organizes the replication fork by interacting via its χ subunit with SSB, and via the three CTDs of the three τ subunits (τ_{CTD}) with three Pol III molecules[60,61]. These interactions may facilitate the recruitment of Pol III to the loaded β-clamp. Key components are listed together with the available PDB codes. In the right panel is shown a structural model of SSB bound to an ssDNA interacting with the DnaX-holo-complex via the flexibly linked C-terminal peptide (blue surface).